

Neutrino oscillations, entanglement and coherence: a quantum field theory study in *real time*

Jun Wu,^{1,*} Jimmy A. Hutasoit,^{2,†} Daniel Boyanovsky,^{1,‡} and Richard Holman^{2,§}

¹*Department of Physics and Astronomy,
University of Pittsburgh, Pittsburgh, PA 15260*

²*Department of Physics, Carnegie Mellon University, Pittsburgh, PA 15213, USA*

(Dated: May 31, 2019)

Abstract

The dynamics of neutrino mixing and oscillations are studied directly in finite *real time* in a model that effectively describes charged current weak interactions. Finite time corrections to the S-matrix result for the appearance and disappearance probabilities are obtained. It is observed that these effects may be of the same order of the S-matrix result in long-baseline appearance experiments. We argue that fundamentally, the S-matrix is ill-suited to describe long-baseline events due to the fact that the neutrino is produced in an entangled state with the charged lepton, which is disentangled by the measurement of the charged lepton near the production site. The appearance and disappearance far-detection process is described from the time evolution of this disentangled “collapsed” state, allowing us to establish the conditions under which factorization of detection rates emerges in long-baseline experiments. Under these conditions the event *rate* at the far detector factorizes in terms of the quantum mechanical probabilities, but the *total* number of events factorizes with a different energy dependence of the oscillatory contribution. We also study the time evolution of the reduced density matrix and show explicitly how oscillations are manifest in the off-diagonal terms, *i.e.*, coherences, as a result of a finite time analysis. Lastly, we study a model for the “GSI anomaly” obtaining the time evolution of the population of parent and daughter particles directly in real time. We confirm that the decay rate of parent and growth rate of daughters do *not* feature oscillatory behavior from interference of mass eigenstates. However, we find an intriguing result that *fluctuations* in the distribution of daughter particles do show oscillations as a consequence of such interference.

PACS numbers: 14.60.Pq;13.15.+g;12.15.Ff

*Electronic address: juw31@pitt.edu

†Electronic address: jhutasoi@andrew.cmu.edu

‡Electronic address: boyan@pitt.edu

§Electronic address: rh4a@andrew.cmu.edu

I. INTRODUCTION

Neutrino masses, mixing and oscillations are the clearest evidence yet of physics beyond the standard model [1–3]. They provide an explanation of the solar neutrino problem [4–6] and have other important phenomenological [1–3, 7–10], astrophysical [5, 11, 12] and cosmological [13] consequences.

In its simplest (and perhaps overly naive) inception, mixing and oscillations of massive neutrinos have been explained by an analogy with a two level system undergoing Rabi-like oscillations between them. Oscillations emerge from the interference of the quantum mechanical states associated with the mass eigenstates (see for example [1–3, 7, 8] and references therein). As simple and compelling as this interpretation is, deeper investigations of this basic paradigm have raised a number of important and fundamental questions [14]. One of these involves the energy and momentum uncertainties [15–18], a topic that is still receiving attention [19–21] (for a recent review see [22]). The recognition that exact energy and momentum conservation prevent oscillations between neutrinos of different masses [15] has led to the consideration of oscillation experiments in terms of wave-packets [15–17] including the quantum mechanical aspects of production and detection which have been incorporated in the quantum field theoretical framework [22–32].

Previous quantum field theory treatments of mixing and oscillations are S-matrix theoretic in nature, making use of in-out wave-packets spatially localized at the source, or the “near” detector¹, and the far detector [22, 24–30, 32]. However, in all these treatments the S-matrix calculation takes the *interaction time to infinity*, even when in some treatments the initial and final wave packets are defined at finite source and detector times [28, 30, 32]. This incongruity between keeping a finite baseline, with wave packets defined at some initial time at the source and final time at the far detector, and taking the time to infinity in the S-matrix element is usually justified with the statement that time is not measured in appearance or disappearance experiments.

While this is true, it is a practical, but not a fundamental reason for taking the infinite time limit. One can consider a *gedanken* experiment in which clocks at the source (near detector) and far detector are *synchronized* via global positioning satellites and register the detection of the charged leptons at the source and far detectors at the time t_S and t_D , respectively. Obviously, the time difference registered by these clocks $t_D - t_S \sim L$, with L being the baseline². This has uncertainties of the order of the size of the source and detectors as the interaction vertices from which the charged leptons emerge are localized within these regions, (although current resolution of the interaction vertices is much more accurate than this scale).

Furthermore, taking the infinite time limit as in the S-matrix calculation enforces total energy conservation via an overall delta function in the transition amplitude. The transition probability treats the square of this delta function as overall energy conservation multiplied

¹ We are using the term “near” detector to describe measurement apparatus at or nearby the production site, which is used to detect the charged lepton that is produced with the primary neutrino. This is not to be confused with the term near detector that is widely used in the experimental literatures (see for example [33]). The latter is used to detect neutrino at a short baseline.

² In the wave-packet-S-matrix approach advocated in the references above, the wave packets localized at the source and far detectors describe the in and out states prepared at $t_i = -\infty, t_f = \infty$, respectively and are spatially separated by the finite baseline.

by the total time of the interaction, from which an *interaction rate* is extracted by dividing by this time (in the long time limit). However, oscillations arising from quantum mechanical interference have nothing to do with a transition *rate* and in principle do not feature a secular evolution in time.

While there are various quantum field theory calculations of appearance and disappearance processes in the literature (see references above), all of them take the infinite time limit from the outset, leading to overall energy conservation and a transition probability that grows linearly in time. In this article, we will study the quantum field theory of neutrino mixing and oscillations in *real time*, namely keeping a finite time interval between the initial state “prepared” at the source and the final state measured at the (far) detector. Ultimately, we seek a complete space-time description of the dynamics of mixing and oscillations that describes long-baseline experiments.

We obtain the transition matrix element in which neutrinos are produced and detected via charged “leptons”, directly in real time. Comparing with the S-matrix results in the plane wave basis, we discuss how wave packet localization restricts the contributions from different channels and obtain the transition probabilities at finite but long time. For the *appearance probability*, we find that finite time corrections are comparable to or larger than the S-matrix contribution. However, we argue that this formulation is ill-suited to describe long-baseline experiments. Long-baseline experiments involve detection measurements at *two different* times, corresponding to detection of the charged leptons at the near and far detector. The neutrino is produced in an entangled state at the interaction vertex at the source, but the measurement of the charged lepton at the near detector *disentangles* the neutrino. It is this “collapsed” disentangled state that evolves in time and leads to the production of the charged lepton which is measured in the far detector.

We then obtain the near and far detector event rates from the detailed evolution of the entangled state, disentanglement at the near detector and further evolution to the far detector. We discuss under which circumstances the factorization of the processes is valid. We also discuss in detail under what circumstances the usual quantum mechanical description is valid. The real-time analysis of disentanglement and coherence shows that this is the case provided the neutrino state is disentangled on time scales much shorter than the oscillation scale. This analysis also makes manifest the compatibility with energy conservation.

One of the most fascinating aspects of mixing and oscillations of ultrarelativistic neutrinos is that they provide a remarkable manifestation of *macroscopic quantum coherence* over unprecedented long distance and time scales. Whereas in condensed matter systems macroscopic quantum coherence is maintained over mesoscopic scales, long baseline disappearance and appearance experiments probe the coherence of the neutrino states over scales of hundreds of kilometers.

More recently, a discussion of coherence aspects of neutrinos [21, 26, 34] recognized that neutrinos produced by the decay of a parent particle are *entangled* with the daughter charged lepton, but the treatment [21, 26] invokes the infinite time limit. We analyze the time evolution of the reduced density matrix for the neutrino and show that keeping finite time allows us to understand the time evolution of the population and coherences. We establish that indeed coherence, as determined by the off-diagonal density matrix elements in the mass basis is maintained up to the oscillation time scale.

Another clear evidence of the fact that the theory of neutrino oscillations is far from being understood at a fundamental level is found in recent controversies regarding the recoilless emission and detection of neutrinos (Mossbauer neutrinos) [35–37]. Yet another can be

found in the controversial interpretation of the GSI anomaly [20, 38–41], namely, periodic modulations in the K-electron capture and β^+ decay rate [42] in terms of quantum beats resulting from the mixing of neutrino mass eigenstates and their interference in the final state [43–45]. In this article, we carry out a real time analysis of the decay of a parent particle into a daughter particle and a “flavor” neutrino. We show that both the decay rate of the parent, and growth rate of the daughter populations *do not feature oscillations* as a consequence of mixing and establish unambiguously the reasons. We therefore conclude that the “GSI-anomaly” cannot be explained by the interference of mass eigenstates in the final state. However, we find an intriguing phenomenon in which the *square* of the growth rate of the daughter particle *does feature* oscillations as a consequence of this interference, a situation which we interpret as *fluctuations in time*, but whose relationship to the GSI anomaly is far from clear.

II. A MODEL OF “NEUTRINO” OSCILLATIONS

The goal of this work is to study the dynamics of mixing and oscillation of neutrinos in quantum field theory but in a finite time interval. In order to exhibit the main results in a clear and simpler manner, we introduce a bosonic model that describes mixing, oscillations and charged current weak interactions reliably without the complications associated with fermionic and gauge fields. We can do so because the technical complications associated with spinors and gauge fields are irrelevant to the physics of mixing and oscillations, as is obviously manifest in meson mixing. Our model is defined by the following Lagrangian density

$$\mathcal{L} = \mathcal{L}_0[W, l_\alpha] + \mathcal{L}_0[\nu_\alpha] + \mathcal{L}_{\text{int}}[W, l_\alpha, \nu_\alpha] \quad ; \quad \alpha = e, \mu \quad (2.1)$$

with

$$\mathcal{L}_0[\nu] = \frac{1}{2} [\partial_\mu \Psi^T \partial^\mu \Psi - \Psi^T \mathbb{M} \Psi] \quad , \quad (2.2)$$

where Ψ is a flavor doublet representing the neutrinos

$$\Psi = \begin{pmatrix} \nu_e \\ \nu_\mu \end{pmatrix} \quad , \quad (2.3)$$

and \mathbb{M} is the mass matrix

$$\mathbb{M} = \begin{pmatrix} m_{ee} & m_{e\mu} \\ m_{e\mu} & m_{\mu\mu} \end{pmatrix} \quad . \quad (2.4)$$

The interaction Lagrangian is similar to the charged current interaction of the standard model, namely

$$\mathcal{L}_{\text{int}}(\vec{x}, t) = g W(\vec{x}, t) \left[l_e(\vec{x}, t) \nu_e(\vec{x}, t) + l_\mu(\vec{x}, t) \nu_\mu(\vec{x}, t) \right] \quad , \quad (2.5)$$

where g is the coupling constant. $W(x)$ represents the vector boson, or alternatively the pion field, and l_α , $\alpha = e, \mu$ the two charged leptons. The mass matrix is diagonalized by a unitary transformation

$$U^{-1}(\theta) \mathbb{M} U(\theta) = \begin{pmatrix} m_1 & 0 \\ 0 & m_2 \end{pmatrix} \quad ; \quad U(\theta) = \begin{pmatrix} \cos \theta & \sin \theta \\ -\sin \theta & \cos \theta \end{pmatrix} \quad . \quad (2.6)$$

In terms of the doublet of mass eigenstates, the flavor doublet can be expressed as

$$\begin{pmatrix} \nu_e \\ \nu_\mu \end{pmatrix} = U(\theta) \begin{pmatrix} \nu_1 \\ \nu_2 \end{pmatrix}. \quad (2.7)$$

This bosonic model clearly describes charged current weak interactions reliably as it includes all the relevant aspects of mixing and oscillations.

We consider “neutrino” oscillation experiments following the interaction processes illustrated in Fig. 1,

$$W \rightarrow l_\alpha + \nu_\alpha \rightsquigarrow \begin{cases} W + l_\beta & , \beta \neq \alpha & \text{appearance} \\ W + l_\alpha & & \text{disappearance} \end{cases}. \quad (2.8)$$

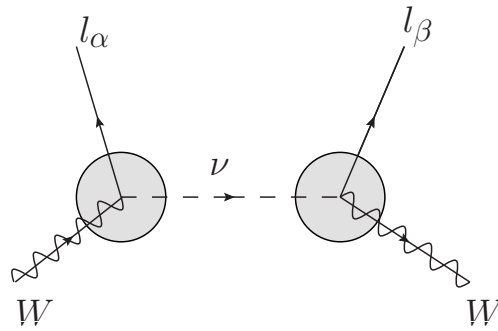


FIG. 1: Typical experiment in which the charged leptons are measured at a near and far detector and the neutrino is an intermediate state.

In a quantum field theory calculation of the transition amplitudes, neutrinos propagating between the production and detection regions are considered as intermediate particles [16, 22–28, 30, 32] and are described by a (free field) propagator.

In order to extract the main physical aspects and new results in the clearest manner, we study the time evolution in terms of *plane waves*, postponing the necessarily more technical discussion in terms of wave-packets to a follow up article. However, to set the stage to the next step that includes such formulation, we revisit some aspects related to wave packet localization that are relevant for the present discussion.

For a wave packet description we consider the initial and final $W, l_{e,\mu}$ states to be described by wave packets. Specifically, we consider the following type of spatially localized wave functions

$$f(\vec{x}, \vec{X}; \vec{p}) = N e^{-\frac{(\vec{x}-\vec{X})^2}{2\sigma^2}} e^{-i\vec{p}\cdot\vec{x}} \quad (2.9)$$

where N is a normalization factor, $\vec{X}_{S,D}$ is the center of the wave packet for source and detection, respectively. σ is the localization length of the wavepacket, which might be a nuclear scale or a *macroscopic* scale of the order of the size of the detector and production regions. We will only require that $\sigma \ll |\vec{X}_D - \vec{X}_S|$. The spatial Fourier transform of these wavepackets is

$$\tilde{f}(\vec{P}, \vec{p}; \vec{X}) = \int d^3x e^{i\vec{P}\cdot\vec{x}} f(\vec{x}, \vec{X}; \vec{p}) = \mathcal{N} e^{-\frac{1}{2}(\vec{P}-\vec{p})^2\sigma^2} e^{i(\vec{P}-\vec{p})\cdot\vec{X}}; \quad \mathcal{N} = \left[\frac{\sigma}{\sqrt{2\pi}} \right]^3. \quad (2.10)$$

The normalization factor in Fourier space, \mathcal{N} , has been chosen so that in the macroscopic limit $\sigma \rightarrow \infty$, the wavepacket has a definite momentum $\tilde{f}(\vec{p}, \vec{k}; \vec{X}) \rightarrow \delta^{(3)}(\vec{p} - \vec{k})$. The initial and final quantum states are localized at the source (\vec{X}_S) or detection (\vec{X}_D) sites and are described by wavepackets that feature mean momenta $\vec{K}_S, \vec{K}_D; \vec{P}_S, \vec{P}_D$ respectively

$$\begin{aligned} |\widetilde{W}(S)\rangle &\equiv |\widetilde{W}(\vec{K}_S; \vec{X}_S)\rangle = \int d\vec{k}_S \tilde{f}(\vec{K}_S, \vec{k}_S; \vec{X}_S) |W(\vec{k}_S)\rangle, \\ |\widetilde{W}(D)\rangle &\equiv |\widetilde{W}(\vec{K}_D; \vec{X}_D)\rangle = \int d\vec{k}_D \tilde{f}(\vec{K}_D, \vec{k}_D; \vec{X}_D) |W(\vec{k}_D)\rangle, \\ |\widetilde{l}_\alpha(S)\rangle &\equiv |\widetilde{l}_\alpha(\vec{P}_S; \vec{X}_S)\rangle = \int d\vec{p}_S \tilde{f}(\vec{P}_S, \vec{p}_S; \vec{X}_S) |l_\alpha(\vec{p}_S)\rangle, \\ |\widetilde{l}_\alpha(D)\rangle &\equiv |\widetilde{l}_\alpha(\vec{P}_D; \vec{X}_D)\rangle = \int d\vec{p}_D \tilde{f}(\vec{P}_D, \vec{p}_D; \vec{X}_D) |l_\alpha(\vec{p}_D)\rangle, \end{aligned} \quad (2.11)$$

where the quantum states $|W(\vec{k}_S)\rangle, |W(\vec{p}_D)\rangle, |l_\alpha(\vec{k}_S)\rangle, |l_\alpha(\vec{p}_D)\rangle$ on the right hand side of Eq. (2.11) are *plane wave* single particle states, which are the eigenstates of the non-interacting Hamiltonian. In term of these localized states, the appearance and disappearance transition amplitudes *for wave packets* prepared and detected at the source (near detector) at an initial time t_i and detected at a far detector at a final time t_f are given by

$$\tilde{\mathcal{A}}_{\alpha \rightarrow \beta} = \langle \widetilde{W}(D), \widetilde{l}_\beta(D); \widetilde{l}_\alpha(S) | e^{-i\hat{H}(t_f - t_i)} | \widetilde{W}(S) \rangle, \quad (2.12)$$

$$\tilde{\mathcal{A}}_{\alpha \rightarrow \alpha} = \langle \widetilde{W}(D), \widetilde{l}_\alpha(D); \widetilde{l}_\alpha(S) | e^{-i\hat{H}(t_f - t_i)} | \widetilde{W}(S) \rangle, \quad (2.13)$$

where D and S label the states localized in the detection and source regions, respectively. The respective probabilities are

$$\mathcal{P}_{\alpha \rightarrow \beta} = |\tilde{\mathcal{A}}_{\alpha \rightarrow \beta}|^2 \quad \text{and} \quad \mathcal{P}_{\alpha \rightarrow \alpha} = |\tilde{\mathcal{A}}_{\alpha \rightarrow \alpha}|^2. \quad (2.14)$$

The transition amplitudes between the initial and final localized states are given by

$$\begin{aligned} \langle \widetilde{W}(D), \widetilde{l}_\beta(D); \widetilde{l}_\alpha(S) | e^{-i\hat{H}(t_f - t_i)} | \widetilde{W}(S) \rangle &= \int d\vec{k}_S d\vec{p}_S d\vec{p}_D d\vec{k}_D e^{-iE_f t_f} \mathcal{A}_{\alpha \rightarrow \beta} e^{iE_i t_i} \tilde{f}^*(\vec{K}_D, \vec{k}_D; \vec{X}_D) \\ &\quad \tilde{f}^*(\vec{P}_S, \vec{p}_S; \vec{X}_S) \tilde{f}(\vec{P}_D, \vec{p}_D; \vec{X}_D) \tilde{f}(\vec{K}_S, \vec{k}_S; \vec{X}_S), \end{aligned} \quad (2.15)$$

where

$$E_i = E_{\vec{k}_S}^W; \quad E_f = E_{\vec{k}_D}^W + E_{\vec{p}_D}^l + E_{\vec{p}_S}^l, \quad (2.16)$$

and

$$\mathcal{A}_{\alpha \rightarrow \beta} = \langle W(\vec{k}_D), l_\beta(\vec{p}_D); l_\alpha(\vec{p}_S) | U(t_f, t_i) | W(\vec{k}_S) \rangle \quad (2.17)$$

is the usual transition matrix element in terms of plane waves eigenstates of the non-interacting Hamiltonian in the interaction picture. To obtain the above expressions we have passed to the interaction picture by writing

$$e^{-i\hat{H}(t_f - t_i)} = e^{-iH_0 t_f} U(t_f, t_i) e^{iH_0 t_i}, \quad (2.18)$$

with the time evolution operator in the interaction picture

$$U(t_f, t_i) = e^{iH_0 t_f} e^{-i\hat{H}(t_f - t_i)} e^{-iH_0 t_i} = T e^{i \int_{t_i}^{t_f} d^3 x dt \mathcal{L}_{\text{int}}(\vec{x}, t)}, \quad (2.19)$$

and we have also used the fact that the initial and final quantum states in (2.17) are free single particle plane wave eigenstates of the non-interacting Hamiltonian H_0 with $E_k^W = \sqrt{k^2 + M_W^2}$, $E_p^l = \sqrt{p^2 + m_l^2}$.

These are the main ingredients in the appearance and disappearance transition probabilities in terms of the localized wave packets. In the limit when the localization length goes to infinity $\sigma \rightarrow \infty$ with the normalization (2.10), the functions \tilde{f} become delta functions in momentum and the localized states become simple plane wave states. In what follows we will obtain the transition matrix element $\mathcal{A}_{\alpha \rightarrow \beta}$ (2.17) up to second order in the interaction.

III. APPEARANCE AND DISAPPEARANCE AMPLITUDES AND PROBABILITIES

A. Localization and suppression of crossed channel contributions

Up to second order in the coupling g the matrix element $\mathcal{A}_{\alpha \rightarrow \beta}$ features the contributions depicted in figs. (2a,b) respectively. If the lepton at the production vertex were in-coming, Fig. (a) would be the equivalent of an s-channel and Fig. (b) of a t-channel contribution. We refer to these as “s” and “t” channel contributions respectively for the remainder of the discussion.

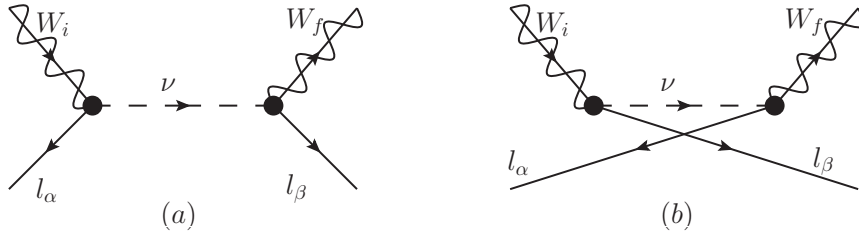


FIG. 2: Feynman diagrams that contribute to $\mathcal{A}_{\alpha \rightarrow \beta}$ up to second order. Diagram (a) corresponds to the “s-channel” and (b) to the “t-channel.”

For the “s” and “t”-channels we find respectively

$$\mathcal{A}_{\alpha \rightarrow \beta}^{(s)} = -g^2 \Pi \int_{t_i}^{t_f} dt_1 dt_2 \int d^3 x_1 d^3 x_2 e^{i(E_{\vec{k}_D}^W t_1 - \vec{k}_D \cdot \vec{x}_1)} e^{i(E_{\vec{p}_D}^l t_1 - \vec{p}_D \cdot \vec{x}_1)} e^{i(E_{\vec{p}_S}^l t_2 - \vec{p}_S \cdot \vec{x}_2)} e^{-i(E_{\vec{k}_S}^W t_2 - \vec{k}_S \cdot \vec{x}_2)} \langle 0 | T(\nu_\beta(x_1) \nu_\alpha(x_2)) | 0 \rangle, \quad (3.1)$$

and

$$\mathcal{A}_{\alpha \rightarrow \beta}^{(t)} = -g^2 \Pi \int_{t_i}^{t_f} dt_1 dt_2 \int d^3 x_1 d^3 x_2 e^{i(E_{\vec{k}_D}^W t_1 - \vec{k}_D \cdot \vec{x}_1)} e^{i(E_{\vec{p}_S}^l t_1 - \vec{p}_S \cdot \vec{x}_1)} e^{i(E_{\vec{p}_D}^l t_2 - \vec{p}_D \cdot \vec{x}_2)} e^{-i(E_{\vec{k}_S}^W t_2 - \vec{k}_S \cdot \vec{x}_2)} \langle 0 | T(\nu_\beta(x_1) \nu_\alpha(x_2)) | 0 \rangle, \quad (3.2)$$

where for disappearance $\alpha = \beta$, for appearance $\alpha \neq \beta$, and

$$\Pi = \left[\frac{1}{16 V^4 E_{\vec{k}_S}^W E_{\vec{k}_D}^W E_{\vec{p}_S}^l E_{\vec{p}_D}^l} \right]^{\frac{1}{2}}. \quad (3.3)$$

The transition matrix elements $\tilde{\mathcal{A}}_{\alpha \rightarrow \beta}$ between the initial and final localized states are obtained from the $\mathcal{A}_{\alpha \rightarrow \beta}$ matrix elements above by convolution with the wave packets describing these localized states (see Eq. 2.15). In order to understand the features associated with the localization, we consider wave packets with a *macroscopic* localization scale $\sigma \ll |\vec{X}_D - \vec{X}_S|$ of the order of the size of the detectors, in which case the wave packets are nearly plane waves and we can approximate $p_{S,D} \simeq P_{S,D}$, $k_{S,D} \simeq K_{S,D}$ in the arguments. For the s-channel we obtain

$$\tilde{\mathcal{A}}_{\alpha \rightarrow \beta}^{(s)} \propto e^{-\frac{(\vec{x}_1 - \vec{X}_S)^2}{\sigma^2}} e^{-\frac{(\vec{x}_2 - \vec{X}_D)^2}{\sigma^2}}, \quad (3.4)$$

whereas for the t-channel contribution we obtain

$$\tilde{\mathcal{A}}_{\alpha \rightarrow \beta}^{(t)} \propto e^{-\frac{(\vec{x}_1 - \vec{X}_S)^2}{2\sigma^2}} e^{-\frac{(\vec{x}_1 - \vec{X}_D)^2}{2\sigma^2}} e^{-\frac{(\vec{x}_2 - \vec{X}_S)^2}{2\sigma^2}} e^{-\frac{(\vec{x}_2 - \vec{X}_D)^2}{2\sigma^2}}. \quad (3.5)$$

Therefore, while for the s-channel the x_1, x_2 integrals factor out, the t-channel contribution obviously vanishes for $|\vec{X}_D - \vec{X}_S| \gg \sigma$. In other words, a localization of the initial and final states even over *macroscopic* scales, as long as $\sigma \ll |\vec{X}_D - \vec{X}_S|$, ensures that the “t”-channel contribution depicted in the second Feynman diagram Fig. 2 vanishes.

B. Amplitudes and probabilities for plane waves

In what follows we consider only the “s”-channel contribution and focus solely on studying the transition amplitudes for *plane waves*, postponing to forthcoming work a full space-time description of the production-detection process.

The plane wave transition amplitudes $\mathcal{A}_{\alpha \rightarrow \beta}$ are given by

$$\begin{aligned} \mathcal{A}_{\alpha \rightarrow \beta} = -g^2 \Pi \int_{t_i}^{t_f} dt_1 dt_2 \int d^3 x_1 d^3 x_2 & e^{i(E_D^W t_1 - \vec{k}_D \cdot \vec{x}_1)} e^{i(E_D^l t_1 - \vec{p}_D \cdot \vec{x}_1)} e^{i(E_S^l t_2 - \vec{p}_S \cdot \vec{x}_2)} \\ & e^{-i(E_S^W t_2 - \vec{k}_S \cdot \vec{x}_2)} \langle 0 | T(\nu_\beta(x_1) \nu_\alpha(x_2)) | 0 \rangle. \end{aligned} \quad (3.6)$$

Here

$$\langle 0 | T(\nu_\beta(x_1) \nu_\alpha(x_2)) | 0 \rangle = \sum_{j=1,2} U_{\beta j} U_{j\alpha} \langle 0 | T(\nu_j(x_1) \nu_j(x_2)) | 0 \rangle, \quad (3.7)$$

where U_{ab} are the matrix elements of the matrix U given in Eq. (2.6), and

$$\langle 0 | T(\nu_j(x_1) \nu_j(x_2)) | 0 \rangle = i \int \frac{d^3 p}{(2\pi)^3} \int \frac{d\omega}{2\pi} \frac{e^{i\vec{p} \cdot (\vec{x}_1 - \vec{x}_2)} e^{-i\omega(t_1 - t_2)}}{\omega^2 - \Omega_j^2 + i\epsilon}; \quad j = 1, 2 \quad (3.8)$$

are the propagators for the mass eigenstates, with

$$\Omega_j^2 = p^2 + m_j^2. \quad (3.9)$$

Here, E_D^W (E_D^l) and \vec{k}_D (\vec{p}_D) label the energy and momentum of the vector boson (charged lepton) at the detection region, while E_S^W (E_S^l) and \vec{k}_S (\vec{p}_S) label those of the production region.

The spatial integrals over \vec{x}_1 and \vec{x}_2 yield the usual spatial momentum conservation $(2\pi)^3 \delta(\vec{p} - \vec{k}_D - \vec{p}_D)$ and $(2\pi)^3 \delta(\vec{k}_S - \vec{p}_S - \vec{p})$, respectively, leading to an overall momentum

conservation in the amplitudes $\mathcal{A}_{\alpha \rightarrow \beta}$ for plane waves. In the transition amplitude for wave packets total momentum conservation is smeared by the wave packet extension.

The integrals over the finite time intervals

$$I = \int_{t_i}^{t_f} dt_1 e^{i(E_D - \omega)t_1} \int_{t_i}^{t_f} dt_2 e^{-i(E_S - \omega)t_2} \quad ; \quad E_S = E_{\vec{k}_S}^W - E_{\vec{p}_S}^l \quad ; \quad E_D = E_{\vec{k}_D}^W + E_{\vec{p}_D}^l \quad (3.10)$$

require a careful treatment. In S-matrix theory, $t_i \rightarrow -\infty$; $t_f \rightarrow \infty$ and the integrals require an adiabatic switching-on convergence factor. We want to analyze this long-time limit to establish contact with the S-matrix results. It proves convenient to write

$$t_f = \frac{T}{2} + \frac{t}{2} \quad ; \quad t_i = \frac{T}{2} - \frac{t}{2} \quad (3.11)$$

and to introduce an adiabatic convergence factor in the integrals

$$I = \lim_{\delta \rightarrow 0^+} e^{i\Delta E \frac{T}{2}} \int_{-\frac{t}{2}}^{\frac{t}{2}} e^{i(E_D - \omega)t_1} e^{-\delta|t_1|} dt_1 \int_{-\frac{t}{2}}^{\frac{t}{2}} e^{-i(E_S - \omega)t_2} e^{-\delta|t_2|} dt_2, \quad (3.12)$$

where

$$\Delta E = E_D - E_S = E_f - E_i, \quad (3.13)$$

and the initial and final energies, E_i and E_f , are defined in Eq. (2.16). We find

$$\int_{-\frac{t}{2}}^{\frac{t}{2}} e^{i(E - \omega)t_1} e^{-\delta|t_1|} dt_1 = 2\pi \delta(E - \omega) + 2\mathcal{S}[(E - \omega); t], \quad (3.14)$$

where the function (distribution)

$$\mathcal{S}[(E - \omega); t] = - \lim_{\delta \rightarrow 0^+} \int_{\frac{t}{2}}^{\infty} \cos[(E - \omega)t_1] e^{-\delta|t_1|} dt_1 \quad (3.15)$$

has the following behavior

$$\lim_{t \rightarrow \infty} \mathcal{S}[(E - \omega); t] = 0 \quad ; \quad \lim_{t \rightarrow 0} \mathcal{S}[(E - \omega); t] = -\pi \delta(E - \omega). \quad (3.16)$$

For a finite time interval and taking first the limit $\delta \rightarrow 0^+$, it follows from (3.14) that

$$\pi \delta(E - \omega) + \mathcal{S}[(E - \omega); t]_{\delta \rightarrow 0^+} \equiv \frac{\sin[(E - \omega)\frac{t}{2}]}{(E - \omega)}. \quad (3.17)$$

We also gather the following useful results

$$\begin{aligned} \lim_{\delta \rightarrow 0^+} \frac{e^{i(\omega - E + i\delta)\frac{t}{2}}}{i(\omega - E + i\delta)} &= - \lim_{\delta \rightarrow 0^+} \int_{\frac{t}{2}}^{\infty} e^{i(\omega - E + i\delta)t_1} dt_1, \\ \lim_{\delta \rightarrow 0^+} \frac{e^{-i(\omega - E - i\delta)\frac{t}{2}}}{i(\omega - E - i\delta)} &= - \lim_{\delta \rightarrow 0^+} \int_{\frac{t}{2}}^{\infty} e^{-i(\omega - E - i\delta)t_1} dt_1, \end{aligned} \quad (3.18)$$

which both go to zero at the infinite time limit $t \rightarrow \infty$.

We note that the prefactor $e^{i\Delta E \frac{T}{2}}$ in (3.12) combines with the factor $e^{-i(E_f t_f - E_i t_i)}$ in (2.15) to yield $e^{-i\bar{E}(t_f - t_i)}$ where $\bar{E} = (E_f + E_i)/2$, manifestly displaying time translational invariance.

The plane wave transition amplitudes are then given by

$$\mathcal{A}_{\alpha \rightarrow \beta}(t) = -ig^2 \Pi (2\pi)^3 \delta(\vec{k}_S - \vec{p}_S - \vec{k}_D - \vec{p}_D) \sum_j U_{\beta j} \mathcal{I}[\Omega_j; t] U_{j\alpha}, \quad (3.19)$$

where $\mathcal{I}[\Omega_j; t]$ is given by the dispersive integral

$$\mathcal{I}[\Omega_j; t] = \frac{2}{\pi} \int d\omega \frac{\left\{ \pi \delta(\omega - E_S) + \mathcal{S}[(\omega - E_S); t] \right\} \left\{ \pi \delta(\omega - E_D) + \mathcal{S}[(\omega - E_D); t] \right\}}{\omega^2 - \Omega_j^2 + i\epsilon}, \quad (3.20)$$

and the momentum argument of the frequencies Ω_j is $\vec{p} = \vec{k}_D + \vec{p}_D = \vec{k}_S - \vec{p}_S$.

Before we carry out the ω integral, we note that taking the $t \rightarrow \infty$ limit at this stage yields energy-momentum conservation at each vertex. This yields

$$\mathcal{I}[\Omega_j; t \rightarrow \infty] = \frac{2\pi \delta(E_f - E_i)}{E_S^2 - \Omega_j^2 + i\epsilon}, \quad (3.21)$$

leading to the usual S-matrix result for the transition amplitude for plane wave initial and final states

$$\mathcal{A}_{\alpha \rightarrow \beta}^{(\text{S-mtx})} = -ig^2 \Pi (2\pi)^4 \delta(E_f - E_i) \delta(\vec{k}_S - \vec{p}_S - \vec{k}_D - \vec{p}_D) \sum_j U_{\beta j} \frac{1}{E_S^2 - \Omega_j^2 + i\epsilon} U_{j\alpha}, \quad (3.22)$$

clearly demonstrating that no oscillations occur for plane waves in the infinite time limit.

For a finite time interval, the integration over ω (3.20) is tedious but straightforward. The result is

$$\mathcal{I}[\Omega_j; t] = \frac{D(E_f - E_i; t)}{E_S^2 - \Omega_j^2 + i\epsilon} + \mathcal{H}[\Omega_j; t] + e^{-i\Omega_j t} \mathcal{F}[\Omega_j; t], \quad (3.23)$$

where to simplify notation we have introduced

$$D(E_f - E_i; t) = 2\pi \delta(E_f - E_i) + 2\mathcal{S}[(E_f - E_i); t], \quad (3.24)$$

$$\mathcal{H}[\Omega_j; t] = \frac{-i}{2\Omega_j} \left\{ \frac{e^{i(E_f - E_i + 2i\delta)\frac{t}{2}}}{(E_f - E_i + 2i\delta)} \left[\frac{E_f - E_i}{(\Omega_j + E_S)(\Omega_j + E_D)} \right] + \frac{e^{-i(E_f - E_i - 2i\delta)\frac{t}{2}}}{(E_f - E_i - 2i\delta)} \left[\frac{E_f - E_i}{(\Omega_j - E_S)(\Omega_j - E_D)} \right] \right\} \quad (3.25)$$

and

$$\mathcal{F}[\Omega_j; t] = \frac{i}{2\Omega_j} \left\{ \frac{e^{-i(E_D + E_S - 2i\delta)\frac{t}{2}}}{(E_D + E_S - 2i\delta)} \left[\frac{E_D + E_S}{(\Omega_j + E_S)(\Omega_j + E_D)} \right] + \frac{e^{i(E_D + E_S + 2i\delta)\frac{t}{2}}}{(E_D + E_S + 2i\delta)} \left[\frac{E_D + E_S}{(\Omega_j - E_S)(\Omega_j - E_D)} \right] \right\}. \quad (3.26)$$

In the $t \rightarrow \infty$ limit, the first term in (3.23) gives the S-matrix result. The functions \mathcal{H} and \mathcal{F} only depend on the frequencies Ω_j in the denominators and vanish in the $t \rightarrow \infty$ limit, as can be seen from Eq. (3.18). It is straightforward to show that there are no poles

at $\Omega_j = \pm E_{D,S}$ because the residues vanish, so that both \mathcal{H} and \mathcal{F} must be understood in terms of their principal part.

The disappearance transition amplitude for *plane waves* are then given by

$$\mathcal{A}_{e \rightarrow e} = -ig^2 \Pi (2\pi)^3 \delta(\vec{k}_S - \vec{p}_S - \vec{k}_D - \vec{p}_D) \left[\cos^2 \theta \mathcal{I}[\Omega_1; t] + \sin^2 \theta \mathcal{I}[\Omega_2; t] \right], \quad (3.27)$$

$$\mathcal{A}_{\mu \rightarrow \mu} = -ig^2 \Pi (2\pi)^3 \delta(\vec{k}_S - \vec{p}_S - \vec{k}_D - \vec{p}_D) \left[\sin^2 \theta \mathcal{I}[\Omega_1; t] + \cos^2 \theta \mathcal{I}[\Omega_2; t] \right], \quad (3.28)$$

while the appearance amplitude is given by

$$\mathcal{A}_{e \rightarrow \mu} = ig^2 \Pi (2\pi)^3 \delta(\vec{k}_S - \vec{p}_S - \vec{k}_D - \vec{p}_D) \cos \theta \sin \theta \left[\mathcal{I}[\Omega_1; t] - \mathcal{I}[\Omega_2; t] \right]. \quad (3.29)$$

Taking the limit $t \rightarrow \infty$ in these amplitudes, one recovers the S-matrix result obtained by replacing $\mathcal{I}[\Omega_j; \infty]$ by (3.21), in which case there is no time dependence and no oscillations from interference terms. Instead of taking this limit, we consider a time interval large compared to microscopic times but of the order of the oscillation time corresponding to the experimental situation in which the baseline is just long enough for a few oscillations. For finite time, we can set $\delta \rightarrow 0^+$ in the above expressions, since we have explicitly separated the delta functions and identified which terms vanish in the formal limit $t \rightarrow \infty$.

We would like to emphasize that there is an important distinction between what we do here and the usual S-matrix approach. In the S-matrix approach, the transition amplitude is obtained in the $t \rightarrow \infty$ limit and after taking this limit, one obtains the transition probability. In contrast, we obtain the transition amplitude at finite time t and obtain the probability.

In order to extract the most relevant contributions at long time, we consider the ultra-relativistic limit and write

$$\Omega_1 = \bar{\Omega} - \Delta \quad ; \quad \Omega_2 = \bar{\Omega} + \Delta, \quad (3.30)$$

where

$$\bar{\Omega} = \left[p^2 + \frac{m_1^2 + m_2^2}{2} \right]^{\frac{1}{2}} \quad ; \quad \Delta = \frac{\delta m^2}{4\bar{\Omega}} \quad ; \quad \delta m^2 = m_2^2 - m_1^2, \quad (3.31)$$

taking $\Delta \ll \bar{\Omega}$ as is the case for ultrarelativistic neutrinos. We can then write

$$\begin{aligned} \mathcal{H}[\Omega_j; t] &= \mathcal{H}[\bar{\Omega}; t] + (-1)^j \left[\bar{\Omega} \frac{d\mathcal{H}[\bar{\Omega}; t]}{d\bar{\Omega}} \right] \left(\frac{\delta m^2}{4\bar{\Omega}^2} \right), \\ \mathcal{F}[\Omega_j; t] &= \mathcal{F}[\bar{\Omega}; t] + (-1)^j \left[\bar{\Omega} \frac{d\mathcal{F}[\bar{\Omega}; \frac{t}{2}]}{d\bar{\Omega}} \right] \left(\frac{\delta m^2}{4\bar{\Omega}^2} \right). \end{aligned} \quad (3.32)$$

We consider the realistic situation in which $\delta m^2/\bar{\Omega}^2 \ll 1$ and keep the terms of $\mathcal{O}(\delta m^2/\bar{\Omega}^2)$ *only* in the S-matrix term and in the exponentials $e^{i\Omega_{1,2}t}$, neglecting the small corrections both in \mathcal{H} and \mathcal{F} . The reason for keeping the $\mathcal{O}(\delta m^2/\bar{\Omega}^2)$ correction in the S-matrix contribution will become clear below when we discuss the appearance probability.

We can further define

$$F[\bar{\Omega}; t] = e^{-i\bar{\Omega}t} \mathcal{F}[\bar{\Omega}; t], \quad (3.33)$$

thus simplifying the expressions for the disappearance and appearance amplitudes

$$\begin{aligned} \mathcal{A}_{e \rightarrow e} = & -ig^2 \Pi (2\pi)^3 \delta(\vec{k}_S - \vec{p}_S - \vec{k}_D - \vec{p}_D) \left\{ D(E_f - E_i; t) \left[\frac{\cos^2 \theta}{E_S^2 - \Omega_1^2 + i\epsilon} + \frac{\sin^2 \theta}{E_S^2 - \Omega_2^2 + i\epsilon} \right] \right. \\ & \left. + \mathcal{H}[\bar{\Omega}; t] + F[\bar{\Omega}; t] \left[\cos^2 \theta e^{i\frac{\delta m^2}{4\bar{\Omega}}t} + \sin^2 \theta e^{-i\frac{\delta m^2}{4\bar{\Omega}}t} \right] \right\} + \mathcal{O}\left(\frac{\delta m^2}{\bar{\Omega}^2}\right), \end{aligned} \quad (3.34)$$

$$\begin{aligned} \mathcal{A}_{e \rightarrow \mu} = & ig^2 \Pi (2\pi)^3 \delta(\vec{k}_S - \vec{p}_S - \vec{k}_D - \vec{p}_D) \cos \theta \sin \theta \left\{ D(E_f - E_i; t) \left[\frac{1}{E_S^2 - \Omega_1^2 + i\epsilon} - \frac{1}{E_S^2 - \Omega_2^2 + i\epsilon} \right] \right. \\ & \left. + 2iF[\bar{\Omega}; t] \sin \left[\frac{\delta m^2}{4\bar{\Omega}} t \right] \right\} + \mathcal{O}\left(\frac{\delta m^2}{\bar{\Omega}^2}\right). \end{aligned} \quad (3.35)$$

The amplitude $\mathcal{A}_{\mu \rightarrow \mu}$ can be obtained from (3.34) by the replacement $\sin^2 \theta \leftrightarrow \cos^2 \theta$.

The expressions above clearly exhibit how and where oscillatory interference terms arise in the probabilities. The usual S-matrix result is obtained in the $t \rightarrow \infty$ limit where $D(E_f - E_i; t) \rightarrow 2\pi \delta(E_f - E_i)$ and $F[\bar{\Omega}, t], \mathcal{H}[\bar{\Omega}, t] \rightarrow 0$. It is clear that in this limit, the oscillatory behavior is suppressed and no interference terms can possibly survive in the transition probabilities.

In obtaining the transition probabilities, we recognize two types of oscillatory terms: terms that feature exponentials of the form $e^{\pm i(E_D \pm E_S)t}$ that appear in \mathcal{F} and \mathcal{H} and those of the form $e^{\pm i\delta m^2 t/4\bar{\Omega}}$. The former are fast oscillatory terms on *microscopic* time scales, whereas the latter are slow phases on these time scales and only manifest themselves on much longer time scales, of order of the baseline $t \sim L$. The fast oscillatory terms average out on the (much) longer time scale. *After* obtaining the transition probabilities at a *finite time* t , we discard terms that feature the fast oscillations that average out in the long time limit, akin to what happens in the “rotating wave approximation” in quantum optics [46], and finally take the $\delta \rightarrow 0^+$ limit, obtaining the *plane wave* transition probabilities

$$\begin{aligned} \mathcal{P}_{e \rightarrow e} = & g^4 \Pi^2 V \delta(\vec{k}_S - \vec{p}_S - \vec{k}_D - \vec{p}_D) \left\{ 2\pi t \delta(E_f - E_i) \left| \frac{\cos^2 \theta}{E_S^2 - \Omega_1^2 + i\epsilon} + \frac{\sin^2 \theta}{E_S^2 - \Omega_2^2 + i\epsilon} \right|^2 \right. \\ & + \frac{1}{4\bar{\Omega}^2} \left[\frac{1}{(\bar{\Omega} + E_S)^2 (\bar{\Omega} + E_D)^2} + \frac{1}{(\bar{\Omega} - E_S)^2 (\bar{\Omega} - E_D)^2} \right] \left(1 - \sin^2 2\theta \sin^2 \left[\frac{\delta m^2}{4\bar{\Omega}} t \right] \right) \\ & \left. + \frac{1}{4\bar{\Omega}^2} \left[\frac{1}{(\bar{\Omega} + E_S)(\bar{\Omega} + E_D)} + \frac{1}{(\bar{\Omega} - E_S)(\bar{\Omega} - E_D)} \right]^2 \right\}, \end{aligned} \quad (3.36)$$

$$\begin{aligned} \mathcal{P}_{e \rightarrow \mu} = & g^4 \Pi^2 V (2\pi)^3 \delta(\vec{k}_S - \vec{p}_S - \vec{k}_D - \vec{p}_D) \sin^2 2\theta \\ & \times \left\{ \frac{(2\pi)}{4} t \delta(E_f - E_i) \left| \frac{1}{E_S^2 - \Omega_1^2 + i\epsilon} - \frac{1}{E_S^2 - \Omega_2^2 + i\epsilon} \right|^2 \right. \\ & \left. + \frac{1}{4\bar{\Omega}^2} \left[\frac{1}{(\bar{\Omega} + E_S)^2 (\bar{\Omega} + E_D)^2} + \frac{1}{(\bar{\Omega} - E_S)^2 (\bar{\Omega} - E_D)^2} \right] \sin^2 \left[\frac{\delta m^2}{4\bar{\Omega}} t \right] \right\}. \end{aligned} \quad (3.37)$$

Here, we have neglected contributions of $\mathcal{O}(\delta m^2/\bar{\Omega}^2)$. As before, the disappearance probability $\mathcal{P}_{\mu \rightarrow \mu}$ is obtained from (3.36) by the substitution $\cos^2 \theta \leftrightarrow \sin^2 \theta$.

The first line in the above expressions is the S-matrix result, where we have used $(2\pi\delta(E_f - E_i))^2 \rightarrow (2\pi) t \delta(E_f - E_i)$ as usual. The third line in (3.36) arises from $|\mathcal{H}(\bar{\Omega}; t)|^2$. This term is a direct result of calculating the probability at *finite time* before taking the $t \rightarrow \infty$ limit. The two procedures *do not commute*. On one hand, taking the $t \rightarrow \infty$ limit first results in the vanishing of \mathcal{H} by the averaging of the oscillatory terms (Riemann-Lebesgue lemma). On the other hand, obtaining the probability first and taking the long time limit afterward yields the contribution from the modulus squared of each oscillatory term, leading to the third line in (3.36).

Writing $\Omega_{1,2}$ as in Eqs. (3.30,3.31), it follows that the S-matrix contribution to the appearance probability is

$$\mathcal{P}_{e \rightarrow \mu}^{S\text{-mtx}} \propto \delta(E_f - E_i) \left[\frac{\delta m^2 t}{4\bar{\Omega}} \right] \frac{\delta m^2 \bar{\Omega}}{(E_S^2 - \bar{\Omega}^2)^4}. \quad (3.38)$$

Upon integrating on the final density of states for times such that there are few oscillations, namely $\delta m^2 t / 4\bar{\Omega} \sim 1$, the S-matrix contribution is *much smaller* than the oscillatory terms in the second line of (3.37) because $\delta m^2 \ll \bar{\Omega}^2, E_{S,D}^2$. On the other hand, the S-matrix contribution to the disappearance probability is

$$\mathcal{P}_{e \rightarrow e}^{S\text{-mtx}} \propto t \delta(E_f - E_i) \frac{1}{(E_S^2 - \bar{\Omega}^2)^2}, \quad (3.39)$$

which upon integration over the density of states will dominate over the oscillatory terms in these probabilities for $t \sim t_{osc} \sim 4\bar{\Omega}/\delta m^2$. Thus we see that appearance and disappearance probabilities are *fundamentally* different. For time scales during which oscillation phenomena can be observed, the S-matrix contribution to the disappearance probability dominates while this may not be the case for the appearance probability, as the oscillatory terms emerging at finite time may be comparable to or larger than the S-matrix contributions.

Lastly, we would also like to note that the oscillatory terms feature an energy dependence very different from that of the S-matrix contribution.

C. Which time scale?

An important question emerges from the analysis above. *What is the value of the time t in these probabilities?*

The linear time dependence, a consequence of *total energy* conservation, also emerges in the analysis with wave packets [16, 24–28, 30, 32, 37], where the S-matrix evaluation of the transition probabilities yields a result proportional to t/L^2 where t is the “total reaction time” arising from squaring the delta function associated with overall energy conservation and L is the baseline. The factor $1/L^2$ corresponds to the flux from a localized source.

In a typical S-matrix calculation one divides by t , the “total reaction time,” to obtain a *transition rate*. However, this interpretation needs revision in the case of long-baseline experiments. In these experiments, a charged lepton is measured at the near detector (source) whereas another charged lepton is measured at the far detector. The intermediate neutrino state propagates between these as a wave packet. Therefore, there are two time scales in this

case: the time at which the near-detector measurement of the charged lepton occurs and the time at which the detection of the charged lepton at the far detector occurs. The question of what precisely is the time t in the S-matrix calculation is in principle independent from the wave packet treatment and is an inherent question to the S-matrix formulation of the production, detection and propagation in long-baseline experiments.

There is another problem with the analysis that we have done so far. In the absence of oscillations, dividing by time or taking the time derivative yields identical results. However, in the presence of oscillatory contributions, the transition *rate* must be obtained by taking the *time derivative*. The time derivative of the oscillatory terms featured in the transition probabilities (3.36-3.37) are of order $\delta m^2/\bar{\Omega}$. For the disappearance probabilities, this derivative term is subleading with respect to the S-matrix contribution, but it may be of the same order or larger in the case of the appearance probability, as discussed above.

The question of how to interpret the total time t in the transition probabilities, along with the conceptual differences between appearance and disappearance (insofar as the oscillatory contributions), suggests a re-examination of how these probabilities should be calculated.

It proves illuminating to understand the result above from “old-fashioned” time dependent perturbation theory with a finite time interval t_f, t_i . To this end, we will need the second order matrix element

$$\begin{aligned} \mathcal{A}_{\alpha \rightarrow \beta} = & -g^2 \int d^3x_1 d^3x_2 \int_{t_i}^{t_f} dt_1 \int_{t_i}^{t_1} dt_2 \\ & \langle W(\vec{k}_D), l_\beta(\vec{p}_D); l_\alpha(\vec{p}_S) | W(x_1, t_1) l(x_1, t_1) \nu(x_1, t_1) W(x_2, t_2) l(x_2, t_2) \nu(x_2, t_2) | W(\vec{k}_S) \rangle, \end{aligned} \quad (3.40)$$

where we have suppressed the flavor indices in the interaction for simplicity of notation. We note that in the above expression time is ordered $t_f \geq t_1 > t_2$. There are two Wick contractions corresponding to the processes displayed in Fig. (3). In diagram (3a) the charged lepton at the near detector l_S is created at $t_2 < t_1$, namely *before* the charged lepton at the far detector l_D , whereas Fig. (3b) displays the opposite process in which the charged lepton at the far detector is created *before* the charged lepton at the near detector.

$$\begin{aligned} \mathcal{A}_{\alpha \rightarrow \beta}^{(a)} = & -g^2 \Pi (2\pi)^3 \delta(\vec{k}_S - \vec{p}_S - \vec{k}_D - \vec{p}_D) e^{i\Delta E \frac{T}{2}} \times \\ & \sum_j U_{\alpha j} \frac{1}{2\Omega_j(q)} \left\{ \frac{2i \sin(\Delta E \frac{t}{2})}{(E_s - \Omega_j(q))\Delta E} + \frac{e^{-i\Delta E \frac{t}{2}} - e^{-i\Omega_j t} e^{i(E_D + E_S)\frac{t}{2}}}{(\Omega_j(q) - E_S)(\Omega_j(q) - E_D)} \right\} U_{j\beta}, \end{aligned} \quad (3.41)$$

$$\begin{aligned} \mathcal{A}_{\alpha \rightarrow \beta}^{(b)} = & -g^2 \Pi (2\pi)^3 \delta(\vec{k}_S - \vec{p}_S - \vec{k}_D - \vec{p}_D) e^{i\Delta E \frac{T}{2}} \times \\ & \sum_j U_{\alpha j} \frac{1}{2\Omega_j(q)} \left\{ \frac{-2i \sin(\Delta E \frac{t}{2})}{(E_s + \Omega_j(q))\Delta E} + \frac{e^{i\Delta E \frac{t}{2}} - e^{-i\Omega_j t} e^{-i(E_D + E_S)\frac{t}{2}}}{(\Omega_j(q) + E_S)(\Omega_j(q) + E_D)} \right\} U_{j\beta}, \end{aligned} \quad (3.42)$$

where $\vec{q} = \vec{k}_S - \vec{p}_S$. It is straightforward to confirm that $\mathcal{A}_{\alpha \rightarrow \beta}^{(a)} + \mathcal{A}_{\alpha \rightarrow \beta}^{(b)}$ coincides with the results (3.19, 3.23) at finite time taking $\delta, \epsilon = 0$.

In process (a), the interaction vertex annihilates the W_S in the initial state and creates both a neutrino and the charged lepton $l_{\beta,S}$ at the space-time coordinates (\vec{x}_2, t_2) in a superposition of product Fock states, namely in an *entangled state* [21], and annihilates the neutrino and creates the final lepton $l_{\beta,D}$ at $(\vec{x}_1, t_1 > t_2)$. In process (b), the initial W_S

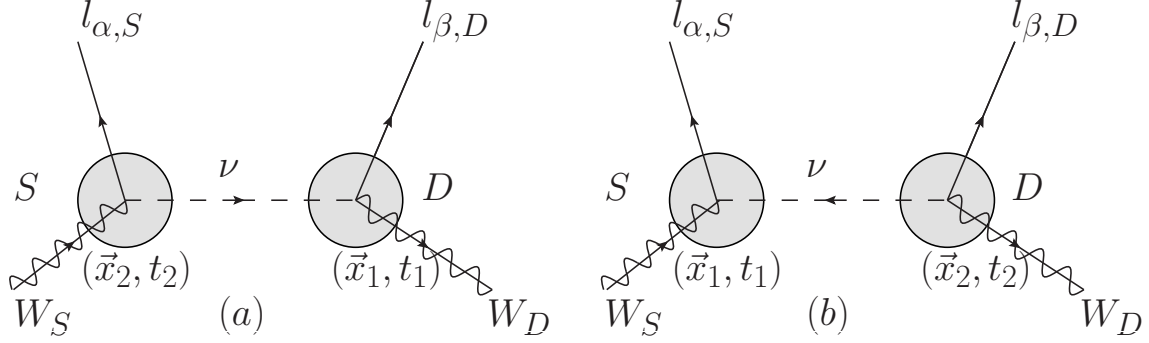


FIG. 3: The two contributions to the transition amplitude (3.40) from the two different Wick contractions. For both diagrams $t_1 > t_2$.

and the final lepton $l_{\beta,S}$ are annihilated and created at (\vec{x}_1, t_1) respectively and the neutrino and $W_D, l_{\alpha,D}$ are created at (\vec{x}_2, t_2) , with the time ordering $t_1 > t_2$. The combination of both contributions yields the time ordered product as usual. However, for a long-baseline experiment when the size of the near and far detectors are much smaller than the distance between them, these processes should *not* contribute on equal footing: the charged lepton produced at the source (near detector) will be detected *much earlier* than the charged lepton produced at the far detector.

A somewhat extreme example which can illustrate the point is SN1987a in the Large Magellanic Cloud. The charged leptons produced in the explosion along with the concomitant neutrinos are trapped, or “detected,” in the optically thick medium, whereas the neutrinos produced at the source are detected at a distance ~ 51 kpc away from the production region. The detection of the charged lepton in the near detector *disentangles* the quantum state. This suggests that long-baseline experiments actually involve *two* times: the time at which the charged lepton produced with the neutrino is detected in the near detector and the time at which the charged lepton produced by the neutrino is detected in the far detector. Obviously, only the process described by the amplitude $\mathcal{A}_{\alpha \rightarrow \beta}^{(a)}$ above describes this physical situation. However, this amplitude does *not* describe the process of measurement of the charged lepton at the near detector, namely, the *disentanglement* of the charged lepton and the neutrino. The correct description requires addressing the issue of coherence and entanglement.

IV. COHERENCE, ENTANGLEMENT AND OSCILLATIONS

In order to study aspects of coherence we consider a simplified interaction Lagrangian density

$$\mathcal{L}_I = g W e \nu_e = g W e (\cos \theta \nu_1 + \sin \theta \nu_2), \quad (4.1)$$

focusing only on one lepton, which we refer to as the “electron” to simplify the discussion. The full coupling as in Eq. (2.5) can be treated similarly without modifying the main conclusions. Although W may be interpreted as a charged vector boson, the analysis is obviously the same if it describes a pion field.

We can study aspects of coherence by focusing on the Fock state obtained upon evolution of the decaying initial state. We consider a plane-wave Fock initial state $|W(\vec{k})\rangle$ at $t_i = 0$.

By time t , this initial state has evolved into $|W(\vec{k})\rangle e^{-iE_k^W t} + |\Psi_e(t)\rangle$. To lowest order in the interaction we find the second term to be

$$|\Psi_e(t)\rangle = ig e^{-iH_0 t} \int_0^t dt' \int d^3x \left[W(\vec{x}, t') e(\vec{x}, t') (\cos \theta \nu_1(\vec{x}, t') + \sin \theta \nu_2(\vec{x}, t')) \right] |W(\vec{k})\rangle, \quad (4.2)$$

where all the fields are in the interaction picture. Though the field operator W can either annihilate the initial state or create another W particle, the state with two W particles features faster oscillations that will average out. In what follows, we consider only the Fock state resulting from the annihilation, leading to the state

$$\begin{aligned} |\Psi_e(t)\rangle \simeq & \frac{g}{2\sqrt{2V E_k^W}} e^{-iE_k^W t} \sum_{\vec{q}} \left\{ \frac{\sin \theta}{\sqrt{\Omega_{2,\vec{p}} E_q^e}} |\nu_{2,\vec{p}}\rangle |e_{\vec{q}}\rangle \left[\frac{e^{i(E_k^W - E_q^e - \Omega_{2,\vec{p}})t} - 1}{(E_k^W - E_q^e - \Omega_{2,\vec{p}})} \right] \right. \\ & \left. + \frac{\cos \theta}{\sqrt{\Omega_{1,\vec{p}} E_q^e}} |\nu_{1,\vec{p}}\rangle |e_{\vec{q}}\rangle \left[\frac{e^{i(E_k^W - E_q^e - \Omega_{1,\vec{p}})t} - 1}{(E_k^W - E_q^e - \Omega_{1,\vec{p}})} \right] \right\} ; \quad \vec{p} = \vec{k} - \vec{q} \end{aligned} \quad (4.3)$$

in which the electron and the neutrinos are *entangled*³. The neutrino state that is entangled with the muon is obtained from (4.3) by replacing $\cos \theta \rightarrow -\sin \theta$; $\sin \theta \rightarrow \cos \theta$.

A. Unobserved daughter particles: time evolution of the density matrix

If the electrons (or daughter particle in Ref.[21]) are not observed, they can be traced out of the *density matrix* $|\Psi_e(t)\rangle\langle\Psi_e(t)|$. This gives the *reduced* density matrix

$$\begin{aligned} \rho_r(t) &= \text{Tr}_e |\Psi_e(t)\rangle\langle\Psi_e(t)| \\ &= \frac{g^2}{8V E_k^W} \sum_{\vec{q}} \left\{ \frac{\sin^2 \theta}{\Omega_{2,\vec{p}} E_q^e} |\nu_{2,\vec{p}}\rangle\langle\nu_{2,\vec{p}}| \left[\frac{\sin \left((E_k^W - E_q^e - \Omega_{2,\vec{p}}) \frac{t}{2} \right)}{(E_k^W - E_q^e - \Omega_{2,\vec{p}})/2} \right]^2 \right. \\ &\quad + \frac{\cos^2 \theta}{\Omega_{1,\vec{p}} E_q^e} |\nu_{1,\vec{p}}\rangle\langle\nu_{1,\vec{p}}| \left[\frac{\sin \left((E_k^W - E_q^e - \Omega_{1,\vec{p}}) \frac{t}{2} \right)}{(E_k^W - E_q^e - \Omega_{1,\vec{p}})/2} \right]^2 \\ &\quad + \frac{\sin 2\theta}{2E_q^e \sqrt{\Omega_{2,\vec{p}} \Omega_{1,\vec{p}}}} \left[\frac{\sin \left((E_k^W - E_q^e - \Omega_{2,\vec{p}}) \frac{t}{2} \right)}{(E_k^W - E_q^e - \Omega_{2,\vec{p}})/2} \right] \left[\frac{\sin \left((E_k^W - E_q^e - \Omega_{1,\vec{p}}) \frac{t}{2} \right)}{(E_k^W - E_q^e - \Omega_{1,\vec{p}})/2} \right] \\ &\quad \left. \times \left[e^{-i\frac{\delta m^2}{4\Omega} t} |\nu_{2,\vec{p}}\rangle\langle\nu_{1,\vec{p}}| + e^{i\frac{\delta m^2}{4\Omega} t} |\nu_{1,\vec{p}}\rangle\langle\nu_{2,\vec{p}}| \right] \right\} ; \quad \vec{p} = \vec{k} - \vec{q}. \end{aligned} \quad (4.4)$$

This expression contains remarkable information. The function $\sin^2(xt)/x^2$ is the usual “diffraction” function of Fermi’s Golden rule. In the formal long time limit $\sin^2(xt)/x^2 \rightarrow$

³ The result for the wavefunction in Ref. [21] may be understood using a (non-perturbative) Wigner-Weisskopf approximation for the decaying parent particle, replacing $E_W \rightarrow E_W - i\Gamma_W$. Taking $t \gg 1/\Gamma_W$ in the integral replaces the brackets in (4.3) by $1/(E_W - E^e - \Omega_j - i\Gamma_W)$ whose absolute value is proportional to $\delta(E_W - E^e - \Omega_j)/\Gamma_W$.

$\pi t \delta(x)$, the first two terms of the density matrix, which are the diagonal entries in the mass basis, describe the production process of the mass eigenstates. As will be seen below, in the long time limit, the time derivative of these two terms yields the production rate for the mass eigenstates. In the formal $t \rightarrow \infty$ limit, these are the diagonal terms obtained in Ref. [21], where in that reference, the product of delta functions is again understood as the total time elapsed times an energy conserving delta function.

The off-diagonal terms in the last line of (4.4) describe the “coherences” and display the oscillatory phases from the interference of the mass eigenstates. The time dependent factors of the off-diagonal density matrix elements determine the *coherence* between the mass eigenstates and will be a ubiquitous contribution in the real time description of oscillations that follows below. The functions

$$f_{\pm}(x, t; \Delta) = \frac{2 \sin \left[(x \pm \Delta) \frac{t}{2} \right]}{(x \pm \Delta)} \quad ; \quad x = E_k^W - E_q^e - \bar{\Omega}_{\bar{p}} \quad ; \quad \Delta = \frac{\delta m^2}{4\Omega}, \quad (4.5)$$

as functions of x are strongly peaked at $x \pm \Delta = 0$ with height t and width $\sim 2\pi/t$. In the infinite time limit $f_{\pm}(x, t, \Delta) \rightarrow 2\pi \delta(x \pm \Delta)$ and thus, their product would vanish in this limit, leading to the vanishing of the coherence. This is the result obtained in Ref. [21]. However, *at finite time* t , they feature a non-vanishing overlap when $2\Delta \lesssim 2\pi/t$. We recognize this precisely as the condition for oscillations. We note that $t \sim \pi/\Delta$ yields a *macroscopically* large time scale. The functions $f_{\pm}(x, t, \Delta)$ and their products are depicted in Figs. (4,5) for the values $\Delta = 0.1$, $t = 40, 100$, respectively.

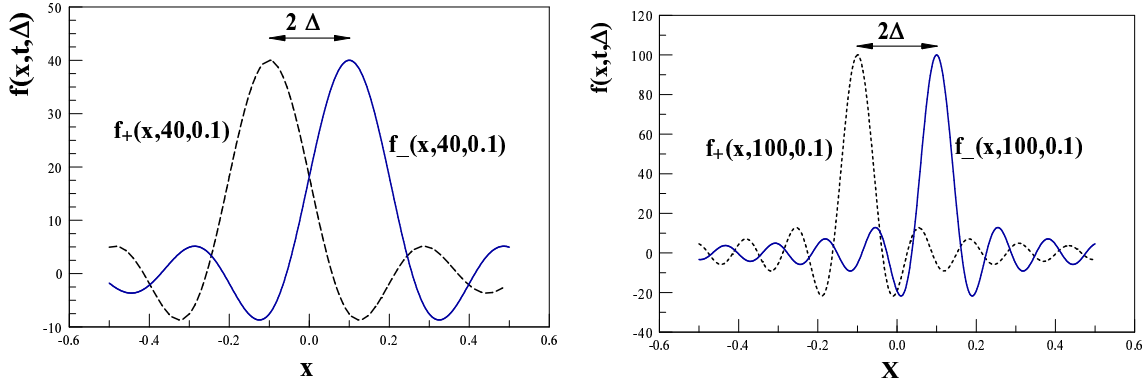


FIG. 4: The functions $f_{\pm}(x, t, \Delta)$ vs. x for $t = 40, 100$, $\Delta = 0.1$

It is straightforward to find

$$\begin{aligned} f_{-}(x, t, \Delta) f_{+}(x, t, \Delta) &= \frac{\sin(\Delta t)}{\Delta} \left[\frac{\sin[(x - \Delta)t]}{(x - \Delta)} + \frac{\sin[(x + \Delta)t]}{(x + \Delta)} \right] \\ &\quad + 2 \frac{\cos(\Delta t)}{\Delta} \left[\frac{\sin^2[(x - \Delta)\frac{t}{2}]}{(x - \Delta)} - \frac{\sin^2[(x + \Delta)\frac{t}{2}]}{(x + \Delta)} \right]. \end{aligned} \quad (4.6)$$

In the long time limit, the terms in the first bracket yield a sum of delta functions at $x = \pm\Delta$. Upon integrating the product of $f_{-}f_{+}$ with functions of compact support, the contribution

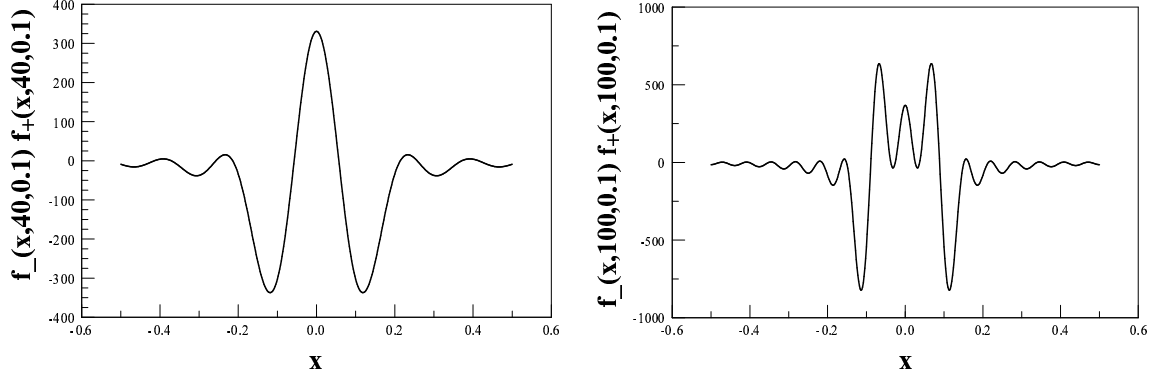


FIG. 5: The products $f_-(x, t, \Delta)f_+(x, t, \Delta)$ vs. x for $t = 40, 100, \Delta = 0.1$

from the second line in (4.6) is negligible in the long time limit. Therefore, the long time limit of f_+f_- can be replaced by

$$f_-(x, t, \Delta)f_+(x, t, \Delta) = \pi \frac{\sin(\Delta t)}{\Delta} \left[\delta(x - \Delta) + \delta(x + \Delta) \right] \quad (4.7)$$

For a large time $t \ll 2\pi/\Delta$, it follows that the product $f_-(x, t, \Delta)f_+(x, t, \Delta) \sim \pi t[\delta(x - \Delta) + \delta(x + \Delta)]$ grows linearly in time but is bound in time. For $t > 2\pi/\Delta$, it oscillates with frequency $2\pi/\Delta$. Therefore, we conclude that upon integration with a smooth density of states, the off-diagonal terms in the density matrix grow linearly in time for $t \ll t_{osc} = 2\pi/\Delta$, but feature a bound oscillatory behavior of frequency Δ for $t \gtrsim 2\pi/\Delta$.

Whereas the diagonal terms, *i.e.*, the first two terms in the reduced density matrix (4.4), are proportional to $4 \sin^2(x \frac{t}{2})/x^2 \rightarrow 2\pi t \delta(x)$, the coherences or the off diagonal terms are linear in time and of the *same order* as the diagonal elements for $t \lesssim t_{osc} = 2\pi/\Delta$, but are of $\mathcal{O}(1/\Delta t)$ and oscillate fast compared to the diagonal terms for $t \gg t_{osc}$. This is similar to the phenomenon observed in the transition probability in the previous section. This behavior is displayed in Fig. (6), where as an example we consider a smooth density of states and the integral

$$I(t, \Delta) = \int_{-\infty}^{\infty} e^{-x^2} f_+(x, t, \Delta) f_-(x, t, \Delta) dx. \quad (4.8)$$

The case $\Delta = 0$ describes either of the diagonal terms and is linearly secular in time. This figure clearly shows the slow oscillations for $t \gtrsim 1/\Delta$.

Therefore, the approximation (4.7) is reliable in the long time limit and upon integration with functions of compact support. We see that for large t , but $t\Delta \ll 1$, $f_+(x, t, \Delta)f_-(x, t, \Delta) \rightarrow \pi t[\delta(x - \Delta) + \delta(x + \Delta)]$ and for $\Delta \rightarrow 0$, the product yields $2\pi t \delta(x)$.

The reduced density matrix (4.4) allows us to obtain the time evolution of the neutrino populations and coherences, namely

$$n_i(\vec{p}, t) = \text{Tr } \rho_r(t) a_i^\dagger(\vec{p}) a_i(\vec{p}) \quad ; \quad \mathcal{C}_{ij}(\vec{p}, t) = \text{Tr } \rho_r(t) a_i^\dagger(\vec{p}) a_j(\vec{p}), \quad i \neq j \quad (4.9)$$

where the annihilation and creation operators are in the Schroedinger picture. In the long time limit and using the results above we find

$$n_1(\vec{p}, t) = t \Gamma_1(\vec{p}) \cos^2 \theta \quad ; \quad n_2(\vec{p}, t) = t \Gamma_2(\vec{p}) \sin^2 \theta, \quad (4.10)$$

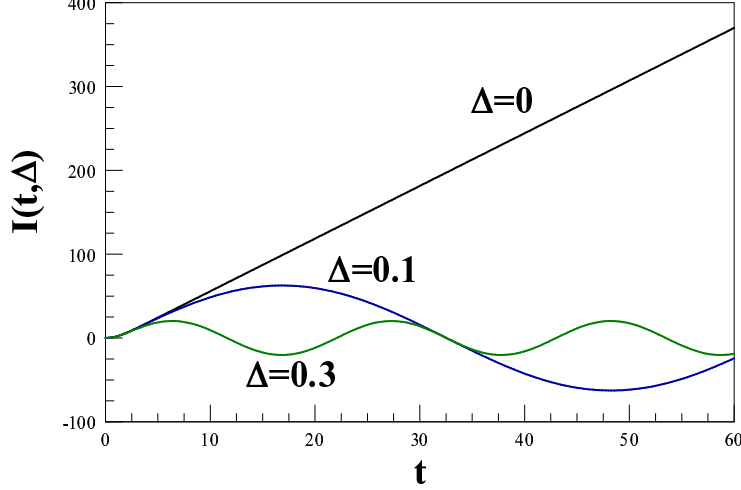


FIG. 6: The integral $I(t, \Delta) = \int_{-\infty}^{\infty} e^{-x^2} f_+(x, t, \Delta) f_-(x, t, \Delta) dx$ vs. t for $\Delta = 0, 0.1, 0.3$

where

$$\Gamma_{1,2} = \frac{2\pi g^2}{8E_k^W} \int \frac{d^3\vec{Q}}{(2\pi)^3 E_{\vec{Q}}^e \Omega_{1,2}} \delta(E_k^W - E_{\vec{Q}}^e - \Omega_{1,2}) \quad (4.11)$$

are the partial widths for the decay of the W into the charged lepton and the neutrino mass eigenstates. Similarly,

$$\begin{aligned} \mathcal{C}_{12}(\vec{p}, t) = \mathcal{C}_{21}^\dagger(\vec{p}, t) &= \frac{2\pi g^2 \sin 2\theta}{32E_k^W} \frac{\sin[t\Delta]}{\Delta} e^{i\Delta t} \\ &\int \frac{d^3\vec{Q}}{(2\pi)^3 E_{\vec{Q}}^e \sqrt{\Omega_1 \Omega_2}} \left[\delta(E_k^W - E_{\vec{Q}}^e - \Omega_1) + \delta(E_k^W - E_{\vec{Q}}^e - \Omega_2) \right]. \end{aligned} \quad (4.12)$$

$dn_i(\vec{p}, t)/dt$ yields the *production rate* of the neutrino mass eigenstates from the decay of the W , and the coherences \mathcal{C}_{ij} are non-vanishing at any finite time. In Ref. [21], these coherences vanish as a consequence of the product of delta functions on the different mass shells of the mass eigenstates. The coherences vanish in the formal infinite time limit because of the oscillatory behavior averages out on time scales $t \gg 1/\Delta$. However, we would like emphasize that on the experimental situation, the time scales involved (or length scales) are of order $1/\Delta$ as these are the scales on which oscillatory phenomena are revealed. Taking $\Omega_1 \sim \Omega_2 \sim \bar{\Omega}$ in the denominators in (4.11,4.12), it follows that

$$\mathcal{C}_{12}(\vec{p}, t) \simeq \frac{\sin 2\theta}{2} \frac{\sin[t\Delta]}{\Delta} e^{i\Delta t} \frac{1}{2} [\Gamma_1 + \Gamma_2]. \quad (4.13)$$

Therefore, the coherences are of the same order of the population terms on time scales $t \leq 1/\Delta$, but average out for $t \gg 1/\Delta$. This clearly shows that coherence is maintained over the oscillation time scale.

B. Disentangling the neutrino: a two-time measurement

As we have discussed previously, a long baseline experiment is actually a *two time measurement*, as the charged lepton produced at the interaction vertex at the *source* is detected by the near detector. This “measurement” of the charged lepton disentangles the neutrinos from the charged lepton in the quantum state (4.3) [21]. The detection of the charged lepton at the near detector projects the quantum state (4.3) at the observation time t_S onto the single particle charged lepton state $e^{-iE_{\vec{Q}}^e t_S} |e_{\vec{Q}}\rangle$ disentangling the neutrino states into the “collapsed” state

$$\begin{aligned}
|\mathcal{V}_e(\vec{Q}, t_S)\rangle &\equiv \langle e_{\vec{Q}} | \Psi(t_S) \rangle e^{iE_{\vec{Q}}^e t_S} \\
&= i \frac{g e^{-iE_S \frac{t_S}{2}}}{2\sqrt{2V E_k^W E_{\vec{Q}}^e}} \left\{ \frac{\sin \theta}{\sqrt{\Omega_{2,\vec{P}}}} |\nu_{2,\vec{P}}\rangle e^{-i\Omega_{2,\vec{P}} \frac{t_S}{2}} \left[\frac{\sin \left[(E_S - \Omega_{2,\vec{P}}) \frac{t_S}{2} \right]}{(E_S - \Omega_{2,\vec{P}})/2} \right] \right. \\
&\quad \left. + \frac{\cos \theta}{\sqrt{\Omega_{1,\vec{P}}}} |\nu_{1,\vec{P}}\rangle e^{-i\Omega_{1,\vec{P}} \frac{t_S}{2}} \left[\frac{\sin \left[(E_S - \Omega_{1,\vec{P}}) \frac{t_S}{2} \right]}{(E_S - \Omega_{1,\vec{P}})/2} \right] \right\}; \\
E_S &= E_k^W - E_{\vec{Q}}^e; \quad \vec{P} = \vec{k} - \vec{Q}
\end{aligned} \tag{4.14}$$

We note that up to a phase the coefficient functions that multiply $|\nu_{1,2}\rangle$ are

$$\frac{\sin \left[(E_S - \Omega_1) \frac{t_S}{2} \right]}{(E_S - \Omega_1)/2}, \quad \frac{\sin \left[(E_S - \Omega_2) \frac{t_S}{2} \right]}{(E_S - \Omega_2)/2}, \tag{4.15}$$

respectively. In the limit $t_S \rightarrow \infty$, these become $2\pi\delta(E_S - \Omega_1)$ and $2\pi\delta(E_S - \Omega_2)$, respectively. Therefore, in this limit, for a fixed E_S , one of the quantum states will be projected out. However, as we insist on keeping a *finite* time interval, we will keep t_S finite.

The state $|\mathcal{V}_e(\vec{Q}, t_S)\rangle$ then evolves forward in time with the full Hamiltonian

$$|\mathcal{V}_e(\vec{Q}, t)\rangle = e^{-iH_0 t} U(t, t_S) e^{iH_0 t_S} |\mathcal{V}_e(\vec{Q}, t_S)\rangle. \tag{4.16}$$

The “free” evolution is obtained by setting to lowest order $U(t, t_S) = 1$, leading to

$$\begin{aligned}
|\mathcal{V}_e(\vec{Q}, t)\rangle &= i \frac{g e^{-iE_S \frac{t_S}{2}}}{2\sqrt{2V E_k^W E_{\vec{Q}}^e}} \left\{ \frac{\sin \theta}{\sqrt{\Omega_{2,\vec{P}}}} |\nu_{2,\vec{P}}\rangle \left[\frac{\sin \left[(E_S - \Omega_{2,\vec{P}}) \frac{t_S}{2} \right]}{(E_S - \Omega_{2,\vec{P}})/2} \right] e^{-i\Omega_{2,\vec{P}} \frac{t_S}{2}} e^{-i\Omega_{2,\vec{P}}(t-t_S)} \right. \\
&\quad \left. + \frac{\cos \theta}{\sqrt{\Omega_{1,\vec{P}}}} |\nu_{1,\vec{P}}\rangle \left[\frac{\sin \left[(E_S - \Omega_{1,\vec{P}}) \frac{t_S}{2} \right]}{(E_S - \Omega_{1,\vec{P}})/2} \right] e^{-i\Omega_{1,\vec{P}} \frac{t_S}{2}} e^{-i\Omega_{1,\vec{P}}(t-t_S)} \right\}.
\end{aligned} \tag{4.17}$$

The phase factors $e^{-i\Omega_j t_S/2}$ multiplying each mass eigenstate are the consequence of the phase build-up during the time evolution from the production vertex until the detection of the charged lepton and the collapse of the wave function. These can be absorbed into the definition of the states $|\nu_{1,2}\rangle$ at the fixed time t_S .

The expression (4.17) features the factors

$$\frac{\sin \left[(E_S - \Omega_j) \frac{t_S}{2} \right]}{(E_S - \Omega_j)/2}, \quad (4.18)$$

which as $t_S \rightarrow \infty$ becomes $2\pi \delta(E_S - \Omega_j)$. These factors, which are a direct consequence of the neutrino state being produced by the decay of the “parent” particle (here the W) into an *entangled* quantum state, distinguish Eq. (4.17) from the familiar quantum mechanical description. These factors emerge from the (approximate) energy conservation at the decay vertex. Again, in the $t_S \rightarrow \infty$ limit, if the energy of the parent particle and the charged lepton are both certain, *only one* of the mass eigenstates will be produced but not both. However, writing $\Omega_{1,2}$ as in Eq. (3.30), it follows that for $t_S \ll 4\bar{\Omega}/\delta m^2$, the width of the “diffraction” functions is *much larger* than the frequency difference Δ and there is a substantial overlap between these “approximate” delta functions (see fig.(4)). Only for $t_S \geq t_{osc} = 2\pi/\Delta$ are the two peaks at $E_S - \bar{\Omega} = \pm\Delta$ actually resolved, whereas for $t_S \ll t_{osc}$, the two peaks are unresolved, “blurred” into one broad peak at $\bar{\Omega}$. Thus, we can use the approximation

$$\frac{\sin \left[(E_S - \Omega_1) \frac{t_S}{2} \right]}{(E_S - \Omega_1)/2} \simeq \frac{\sin \left[(E_S - \Omega_2) \frac{t_S}{2} \right]}{(E_S - \Omega_2)/2} \simeq \frac{\sin \left[(E_S - \bar{\Omega}) \frac{t_S}{2} \right]}{(E_S - \bar{\Omega})/2}, \quad (4.19)$$

for $t_S \ll 2\pi/\Delta$.

To illustrate the validity of the above approximation, let us consider the case in which the typical size of the near detector is a few meters across. In a typical experiment, the charged lepton emerging from the interaction vertex travels this distance within a time scale $t_S \approx 10^{-8}$ s, leading to an energy uncertainty above $\delta E \sim \hbar/t_S \sim 10^{-7}$ eV. Taking as an example $\delta m^2 \sim 10^{-4}$ eV²; $\bar{\Omega} \sim E_S \sim 100$ MeV, it follows that $\delta m^2/\bar{\Omega} \sim 10^{-12}$ eV $\ll \delta E$. Therefore, the detection at the near detector cannot resolve the energy difference between the mass eigenstates and the approximation (4.19) is justified.

Another approximation we can use in (4.14) is $\Omega_1 \simeq \Omega_2 \simeq \bar{\Omega}$, for $\bar{\Omega} \gg \Delta$. Absorbing the phase factors $e^{-i\Omega_j t_S/2}$ into the definition of the states $|\nu_j\rangle$, the time evolved disentangled state is then approximately given by

$$|\mathcal{V}_e(\vec{Q}, t)\rangle \simeq \frac{ig}{[8V E_{\vec{k}}^W E_{\vec{Q}}^e \bar{\Omega}]^{\frac{1}{2}}} \left[\frac{\sin \left[(E_S - \bar{\Omega}) \frac{t_S}{2} \right]}{(E_S - \bar{\Omega})/2} \right] \left\{ \sin \theta |\nu_{2,\vec{P}}\rangle e^{-i\Omega_{2,\vec{P}}(t-t_S)} + \cos \theta |\nu_{1,\vec{P}}\rangle e^{-i\Omega_{1,\vec{P}}(t-t_S)} \right\}, \quad (4.20)$$

for $t_S \ll 2\pi/\Delta$.

The state inside the brackets is identified as the usual quantum mechanical state that is time evolved from the “electron” neutrino state, which is prepared initially at t_S . From this analysis, we see that there are two conditions required for the disentangled neutrino state to be identified with the familiar quantum mechanical state. The two conditions are $\delta m^2/\bar{\Omega}^2 \ll 1$ and $t_S \ll t_{osc} \sim 2\pi\bar{\Omega}/\delta m^2$. The former is always satisfied for neutrinos with $\delta m^2 \sim 10^{-3} - 10^{-4}$ eV², $\bar{\Omega} >$ few MeV, while the latter is fulfilled for near-detection of the charged lepton in long-baseline experiments. The latter condition implies that the neutrino state is *disentangled* before oscillations can occur. In a long-baseline experiment this is achieved if the charged lepton, which is entangled with the neutrino at the production vertex, is measured at the near detector .

C. Transition amplitudes and event rates

The number of charged lepton events with momentum \vec{Q} at the near detector, at time t_S is given by

$$n_e(\vec{Q}, t_S) = \langle \Psi_e(t_S) | a_e^\dagger(\vec{Q}) a_e(\vec{Q}) | \Psi_e(t_S) \rangle = \langle \mathcal{V}_e(\vec{Q}, t_S) | \mathcal{V}_e(\vec{Q}, t_S) \rangle. \quad (4.21)$$

For $t_S \ll t_{osc} = 2\pi/\Delta$ and $\bar{\Omega} \gg \Delta$, using the approximations leading to (4.20), we obtain the differential detection rate at the *near detector*

$$\begin{aligned} (2\pi)^3 \frac{dN_e^{(\text{ND})}}{d^4x d^3\vec{Q}} &= \frac{dn_e(\vec{Q}, t_S)}{dt_S} \\ &= \frac{2g^2}{8VE_k^W E_{\vec{Q}}^e \bar{\Omega}} \frac{\sin \left[(E_S - \bar{\Omega}) t_S \right]}{(E_S - \bar{\Omega})} \\ &\simeq \frac{2\pi g^2}{8VE_k^W E_{\vec{Q}}^e \bar{\Omega}} \delta(E_S - \bar{\Omega}), \end{aligned} \quad (4.22)$$

where at the last step we have replaced the diffraction function by the delta function. This can be justified as follows. For $t_S \sim 10^{-8}$ s, the width of this function (the resolution) in energy is $\sim 10^{-7}$ eV. Since the typical energy in a long-baseline experiment is $\gtrsim 40 - 100$ MeV, the error incurred in replacing the diffraction function by a delta function is smaller than one part in 10^{15} .

We can also obtain the transition amplitude for the disentangled state to produce a final charged lepton and another W particle at the far detector at time t_D , where $t_D - t_S \sim L$ and L is the baseline. It is given by

$$\begin{aligned} \mathcal{A}_{\alpha \rightarrow \beta} &= \langle W(\vec{k}_D), l_\beta(\vec{p}_D) | e^{-iH(t_D - t_S)} | \mathcal{V}_e(\vec{Q}, t_S) \rangle \\ &= e^{-iE_D t_D} \langle W(\vec{k}_D), l_\beta(\vec{p}_D) | U(t_D, t_S) e^{iH_0 t_S} | \mathcal{V}_e(\vec{Q}, t_S) \rangle. \end{aligned} \quad (4.23)$$

The disappearance and appearance amplitudes are then given by

$$\begin{aligned} \mathcal{A}_{e \rightarrow e} &= -g^2 \Pi (2\pi)^3 \delta(\vec{k}_S - \vec{p}_S - \vec{k}_D - \vec{p}_D) \times \\ &\quad \left\{ \frac{\cos^2 \theta}{2\Omega_{1,\vec{P}}} e^{-i\Omega_{1,\vec{P}} \frac{t_D}{2}} \left[\frac{\sin \left[(E_S - \Omega_{1,\vec{P}}) \frac{t_S}{2} \right]}{(E_S - \Omega_{1,\vec{P}})/2} \right] \left[\frac{\sin \left[(E_D - \Omega_{1,\vec{P}}) (t_D - t_S)/2 \right]}{(E_D - \Omega_{1,\vec{P}})/2} \right] \right. \\ &\quad \left. + \frac{\sin^2 \theta}{2\Omega_{2,\vec{P}}} e^{-i\Omega_{2,\vec{P}} \frac{t_D}{2}} \left[\frac{\sin \left[(E_S - \Omega_{2,\vec{P}}) \frac{t_S}{2} \right]}{(E_S - \Omega_{2,\vec{P}})/2} \right] \left[\frac{\sin \left[(E_D - \Omega_{2,\vec{P}}) (t_D - t_S)/2 \right]}{(E_D - \Omega_{2,\vec{P}})/2} \right] \right\} \end{aligned} \quad (4.24)$$

and

$$\begin{aligned} \mathcal{A}_{e \rightarrow \mu} = & -g^2 \Pi (2\pi)^3 \delta(\vec{k}_S - \vec{p}_S - \vec{k}_D - \vec{p}_D) \frac{\sin 2\theta}{2} \times \\ & \left\{ \frac{e^{-i\Omega_{1,\vec{P}} \frac{t_D}{2}}}{2\Omega_{1,\vec{P}}} \left[\frac{\sin \left[(E_S - \Omega_{1,\vec{P}}) \frac{t_S}{2} \right]}{(E_S - \Omega_{1,\vec{P}})/2} \right] \left[\frac{\sin \left[(E_D - \Omega_{1,\vec{P}}) (t_D - t_S)/2 \right]}{(E_D - \Omega_{1,\vec{P}})/2} \right] \right. \\ & \left. - \frac{e^{-i\Omega_{2,\vec{P}} \frac{t_D}{2}}}{2\Omega_{2,\vec{P}}} \left[\frac{\sin \left[(E_S - \Omega_{2,\vec{P}}) \frac{t_S}{2} \right]}{(E_S - \Omega_{2,\vec{P}})/2} \right] \left[\frac{\sin \left[(E_D - \Omega_{2,\vec{P}}) (t_D - t_S)/2 \right]}{(E_D - \Omega_{2,\vec{P}})/2} \right] \right\}, \end{aligned} \quad (4.25)$$

with $\vec{P} = \vec{k}_S - \vec{p}_S$. In these expressions, we have used the same notation as in section (III), where Π is given by (3.3). Implementing the same approximations leading to the factorized state (4.20), namely $\bar{\Omega} \gg \Delta$ and $t_S \Delta \ll 1$, we find the disappearance and appearance probabilities

$$\begin{aligned} \mathcal{P}_{e \rightarrow e}(t_D) = & \left(\frac{g^2 \Pi}{2\bar{\Omega}_{\vec{P}}} \right)^2 (2\pi)^3 V \delta(\vec{k}_S - \vec{p}_S - \vec{k}_D - \vec{p}_D) 2\pi t_S \delta(E_S - \bar{\Omega}_{\vec{P}}) \\ & \left\{ \cos^4 \theta f_+^2(x, t, \Delta) + \sin^4 \theta f_-^2(x, t, \Delta) + 2 \cos^2 \theta \sin^2 \theta \cos(t\Delta) f_+(x, t, \Delta) f_-(x, t, \Delta) \right\}, \\ \mathcal{P}_{e \rightarrow \mu}(t_D) = & \left(\frac{g^2 \Pi}{2\bar{\Omega}_{\vec{P}}} \right)^2 (2\pi)^3 V \delta(\vec{k}_S - \vec{p}_S - \vec{k}_D - \vec{p}_D) 2\pi t_S \delta(E_S - \bar{\Omega}_{\vec{P}}) \frac{\sin^2 2\theta}{4} \\ & \left\{ f_+^2(x, t, \Delta) + f_-^2(x, t, \Delta) - 2 \cos(t\Delta) f_+(x, t, \Delta) f_-(x, t, \Delta) \right\}, \end{aligned} \quad (4.26)$$

where $t = t_D - t_S$ and $x = E_D - \bar{\Omega}_{\vec{P}}$. Here,

$$E_S = E_{\vec{k}_S}^W - E_{\vec{p}_S}^e \quad ; \quad E_D = E_{\vec{k}_D}^W + E_{\vec{p}_D}^l, \quad (4.27)$$

and f_{\pm} are given by Eq. 4.5.

In the long time limit, using $f_{\pm}(x, t, \Delta) \rightarrow 2\pi t \delta(x \pm \Delta)$ and (4.7), we find

$$\begin{aligned} \mathcal{P}_{e \rightarrow e}(t_D) = & \left(\frac{g^2 \Pi}{2\bar{\Omega}_{\vec{P}}} \right)^2 (2\pi)^5 V \delta(\vec{k}_S - \vec{p}_S - \vec{k}_D - \vec{p}_D) t_S \delta(E_S - \bar{\Omega}_{\vec{P}}) \\ & \left\{ \cos^4 \theta t \delta(x + \Delta) + \sin^4 \theta t \delta(x - \Delta) + 2 \cos^2 \theta \sin^2 \theta \frac{\sin(2t\Delta)}{2\Delta} \frac{1}{2} [\delta(x + \Delta) + \delta(x - \Delta)] \right\}, \\ \mathcal{P}_{e \rightarrow \mu}(t_D) = & \left(\frac{g^2 \Pi}{2\bar{\Omega}_{\vec{P}}} \right)^2 (2\pi)^5 V \delta(\vec{k}_S - \vec{p}_S - \vec{k}_D - \vec{p}_D) t_S \delta(E_S - \bar{\Omega}_{\vec{P}}) \frac{\sin^2 2\theta}{4} \\ & \left\{ t \delta(x + \Delta) + t \delta(x - \Delta) - 2 \frac{\sin(2t\Delta)}{2\Delta} \frac{1}{2} [\delta(x + \Delta) + \delta(x - \Delta)] \right\}. \end{aligned} \quad (4.28)$$

where $\vec{P} = \vec{k}_D + \vec{p}_D$.

These transition probabilities are *very different* from the ones obtained in section (III B) at finite time and from those obtained from the S-matrix approach (infinite time limit). They feature the *two* time scales t_S and $t = t_D - t_S$ associated with the measurements at the near and far detector. They also feature energy conserving delta functions associated with the different mass eigenstates.

There is a further simplification when $\bar{\Omega} \gg \Delta$. In this regime, when the probabilities (4.28) are *integrated over a smooth density of states*, the delta functions corresponding to the mass eigenstates yield the density of states at values $E_D = \bar{\Omega} \mp \Delta$. In typical experiments, where $\bar{\Omega} \sim 100 \text{ MeV}$ and $\delta m^2 \sim 10^{-3} \text{ eV}^2$, the density of final states must vary dramatically near $\bar{\Omega}$ to resolve the small interval Δ , with $\Delta/\bar{\Omega} \lesssim 10^{-19}$. Therefore, understanding the probabilities as being integrated with a smooth final density of states insensitive to the mass difference, we can approximate $\delta(x \pm \Delta) \simeq \delta(x)$. In this case, we can approximate the above expressions by

$$\mathcal{P}_{e \rightarrow e}(t_D) = \left(\frac{g^2 \Pi}{2\bar{\Omega}_{\vec{p}}} \right)^2 (2\pi)^5 V \delta(\vec{k}_S - \vec{p}_S - \vec{k}_D - \vec{p}_D) t_S \delta(E_S - \bar{\Omega}_{\vec{p}}) \delta(E_D - \bar{\Omega}_{\vec{p}}) \left\{ t \left[\cos^4 \theta + \sin^4 \theta \right] + 2 \cos^2 \theta \sin^2 \theta \frac{\sin(2t\Delta)}{2\Delta} \right\}, \quad (4.29)$$

$$\mathcal{P}_{e \rightarrow \mu}(t_D) = \left(\frac{g^2 \Pi}{2\bar{\Omega}_{\vec{p}}} \right)^2 (2\pi)^5 V \delta(\vec{k}_S - \vec{p}_S - \vec{k}_D - \vec{p}_D) t_S \delta(E_S - \bar{\Omega}_{\vec{p}}) \delta(E_D - \bar{\Omega}_{\vec{p}}) \frac{\sin^2 2\theta}{2} \left\{ t - \frac{\sin(2t\Delta)}{2\Delta} \right\}. \quad (4.30)$$

The product $\delta(E_S - \bar{\Omega}_{\vec{p}}) \delta(E_D - \bar{\Omega}_{\vec{p}})$ is an *approximate* energy conservation at both production and detection vertices, where we have neglected Δ , which is twice the energy difference between the mass eigenstates. However, even under these justified approximations, the probabilities (4.29,4.30) are very different from those obtained by the S-matrix approach, even after including the finite time corrections discussed in section (III B). They also differ greatly from the transition probabilities from the simple quantum mechanical argument.

Further insight can be gained by obtaining the phase space distribution of the number of charged leptons $l = e, \mu$ at the far detector

$$(2\pi)^3 \frac{dN_l^{FD}}{d^3x d^3\vec{p}_D} = n_l(\vec{p}_D, t_D) = \langle \mathcal{V}_e(\vec{Q}, t_D, t_S) | a_l^\dagger(\vec{p}_D) a_l(\vec{p}_D) | \mathcal{V}_e(\vec{Q}, t_D, t_S) \rangle. \quad (4.31)$$

Here,

$$| \mathcal{V}_e(\vec{Q}, t_D, t_S) \rangle = e^{-iH_0 t_D} U(t_D, t_S) e^{iH_0 t_S} | \mathcal{V}_e(\vec{Q}, t_S) \rangle \quad (4.32)$$

is the neutrino state disentangled at t_S at the near detector and time-evolved until it is detected at the far detector at time t_D . Not surprisingly, since up to order g^2 , the time evolved state contains a single lepton Fock state, we find that

$$(2\pi)^3 \frac{dN_e^{FD}}{d^3x d^3\vec{p}_D} = \mathcal{P}_{e \rightarrow e}(t_D) \quad ; \quad (2\pi)^3 \frac{dN_\mu^{FD}}{d^3x d^3\vec{p}_D} = \mathcal{P}_{e \rightarrow \mu}(t_D), \quad (4.33)$$

with the probabilities $\mathcal{P}_{e \rightarrow e}(t_D)$ and $\mathcal{P}_{e \rightarrow \mu}(t_D)$ are given by (4.29,4.30).

Taking the *time derivative* with respect to t_D , we obtain the differential charged leptons event *rates* at the far detector

$$(2\pi)^3 \frac{dN_e^{FD}}{d^3x dt d^3\vec{p}_D} = \left(\frac{g^2 \Pi}{2\bar{\Omega}_{\vec{p}}} \right)^2 (2\pi)^5 V \delta(\vec{k}_S - \vec{p}_S - \vec{k}_D - \vec{p}_D) t_S \delta(E_S - \bar{\Omega}_{\vec{p}}) \delta(E_D - \bar{\Omega}_{\vec{p}}) \left\{ \cos^4 \theta + \sin^4 \theta + 2 \cos^2 \theta \sin^2 \theta \cos(2t\Delta) \right\}, \quad (4.34)$$

$$(2\pi)^3 \frac{dN_\mu^{FD}}{d^3x dt d^3\vec{p}_D} = \left(\frac{g^2 \Pi}{2\bar{\Omega}_{\vec{p}}} \right)^2 (2\pi)^5 V \delta(\vec{k}_S - \vec{p}_S - \vec{k}_D - \vec{p}_D) t_S \delta(E_S - \bar{\Omega}_{\vec{p}}) \delta(E_D - \bar{\Omega}_{\vec{p}}) \frac{\sin^2 2\theta}{2} \left\{ 1 - \cos(2t\Delta) \right\}. \quad (4.35)$$

Remarkably, these rates can be simply written as

$$(2\pi)^3 \frac{dN_\beta^{FD}}{d^3x dt d^3\vec{p}_D} = (2\pi)^3 \frac{dN_\alpha^{ND}}{d^3x d^3\vec{p}_s} P_{\alpha \rightarrow \beta}(t) d\Gamma_{\nu_\beta \rightarrow W l_\beta}, \quad (4.36)$$

where we have used the expression (4.22) for the differential charged lepton event rate at the near detector and integrated in t_S ,

$$d\Gamma_{\nu_\beta \rightarrow W l_\beta} = \frac{(2\pi)^4 g^2 V}{8V^3 E_{\vec{k}_D}^W E_{\vec{p}_D}^{l_\beta} \bar{\Omega}_{\vec{p}}} \delta(\vec{k}_S - \vec{p}_S - \vec{k}_D - \vec{p}_D) \delta(E_D - \bar{\Omega}_{\vec{p}}) \quad (4.37)$$

is the charged lepton production rate from the reaction $\nu_\beta \rightarrow W l_\beta$ for a *flavor* neutrino of energy $\bar{\Omega}$ and $P_{\alpha \rightarrow \beta}(t)$ are the disappearance ($\alpha = \beta$) or appearance ($\alpha \neq \beta$) *quantum mechanical* transition probabilities.

The remarkable aspect of the final result (4.37) is the *factorization* of the different processes contributing to the far detector event *rate*, namely the number of events at the near detector multiplies the quantum mechanical transition probability which in turn multiplies the production rate at the vertex in the far detector. This factorization is a distinct consequence of the *two time analysis*, of the disentanglement of the neutrino at the near detector, along with the approximations invoked in the resolution of the energy conserving delta functions. We emphasize that the factorization in terms of the quantum mechanical transition probabilities *only* applies to the detection *rate* defined by taking the time derivative. The *total number of events* also factorizes but *not* in terms of the quantum mechanical transition probabilities but in terms of their integral in time, which yields a very different energy dependence.

V. A MODEL FOR THE GSI ANOMALY

Recent experiments at the Experimental Storage Ring (ESR) at GSI in Darmstadt have revealed an unexpected time dependent modulation in the population of daughter ions $^{140}\text{Ce}^{58+}$ from the electron capture decay $^{140}\text{Pr}^{58+} \rightarrow ^{140}\text{Ce}^{58+} + \nu_e$ [42], a phenomenon that has been dubbed the ‘‘GSI anomaly.’’ There have been some works that try to explain

this remarkable time dependent rate of the parent ion decay as an interference between the neutrino mass eigenstates in the decay reaction [20, 42–45]. However, this interpretation has been re-examined and criticized [38–41].

The authors in Refs. [43–45] obtain the decay rate of the parent ion by adding coherently the amplitudes and then obtaining the probabilities, in which case the modulation arises from the interference of the mass eigenstates in the squaring of the amplitudes. The authors in Refs. [38–40] criticize this approach, stating that it is not the amplitudes that must be summed coherently but the probabilities, corresponding to an *incoherent* addition of the contributions from the mass eigenstates. This approach does not lead to any modulation as the amplitudes for the different mass eigenstates do not interfere.

Rather than focusing on either one of these approaches, we analyze the situation *differently*, by obtaining **the time evolution of the population of the parent and daughter particles**. In this approach, we recognize directly the decay rate of the parent particles (or production rate of the daughter) without the necessity to invoke a coherent sum over amplitudes or a sum over probabilities.

We study the time evolution of the populations by modeling the situation in terms of the decay of a parent particle via charged current interactions into a charged lepton and its associated neutrino. The interaction vertex is given by $W e \nu_e$, where we simply take the parent to be the W and the daughter to be the e -charged lepton.

Let us consider an initial parent particle state $|W(\vec{k})\rangle$ that is prepared at time $t = 0$. The evolution of the number of parent and daughter particles is obtained from

$$\begin{aligned} N_W(\vec{k}, t) &= \langle W(\vec{k}) | e^{iHt} a_W^\dagger(\vec{k}) a_W(\vec{k}) e^{-iHt} | W(\vec{k}) \rangle, \\ n_e(\vec{Q}, t) &= \langle W(\vec{k}) | e^{iHt} a_e^\dagger(\vec{Q}) a_e(\vec{Q}) e^{-iHt} | W(\vec{k}) \rangle, \end{aligned} \quad (5.1)$$

where the annihilation and creation operators are in the Schroedinger picture. We note that $e^{-iHt} = e^{-iH_0 t} U(t, 0)$ and that the number operators commute with the free field Hamiltonian. We also note that $U(t, 0)|W\rangle = |W\rangle + |\Psi_e(t)\rangle^{(1)} + |\Psi_e(t)\rangle^{(2)} + \dots$ where

$$|\Psi_e(t)\rangle^{(1)} = ig \int_0^t dt_1 \int d^3x_1 \left[W(\vec{x}_1, t_1) e(\vec{x}_1, t_1) \nu_e(\vec{x}_1, t_1) \right] |W(\vec{k})\rangle, \quad (5.2)$$

and

$$\begin{aligned} |\Psi_e(t)\rangle^{(2)} &= -g^2 \int_0^t dt_1 \int d^3x_1 \int_0^{t_1} dt_2 \int d^3x_2 \left[W(\vec{x}_1, t_1) e(\vec{x}_1, t_1) \nu_e(\vec{x}_1, t_1) \right] \\ &\quad \left[W(\vec{x}_2, t_2) e(\vec{x}_2, t_2) \nu_e(\vec{x}_2, t_2) \right] |W(\vec{k})\rangle, \end{aligned} \quad (5.3)$$

with $\nu_e = \cos \theta \nu_1 + \sin \theta \nu_2$. Since the (entangled) state $|\Psi_e(t)\rangle^{(1)}$ has one daughter particle (electron) and the initial state has none, it is clear that to lowest order, the number of daughter particles is

$$n_e(\vec{Q}, t) = {}^{(1)}\langle \Psi_e(t) | a_e^\dagger(\vec{Q}) a_e(\vec{Q}) | \Psi_e(t) \rangle^{(1)} = \langle \mathcal{V}_e(\vec{Q}, t) | \mathcal{V}_e(\vec{Q}, t) \rangle, \quad (5.4)$$

where $|\mathcal{V}_e(\vec{Q}, t)\rangle$ is the “collapsed” state (4.14). We find the production rate of the daughter particle

$$\frac{dn_e(\vec{Q}, t)}{dt} = \frac{g^2}{8V E_k^W E_Q^e} \left[\frac{\cos^2 \theta}{\Omega_1} \frac{2 \sin [(E_k^W - E_Q^e - \Omega_1)t]}{(E_k^W - E_Q^e - \Omega_1)} + \frac{\sin^2 \theta}{\Omega_2} \frac{2 \sin [(E_k^W - E_Q^e - \Omega_2)t]}{(E_k^W - E_Q^e - \Omega_2)} \right]. \quad (5.5)$$

If at this stage we take the long time limit, using the identity

$$\frac{2 \sin [(E_k^W - E_{\vec{Q}}^e - \Omega_j)t]}{(E_k^W - E_{\vec{Q}}^e - \Omega_j)} \rightarrow 2\pi\delta(E_k^W - E_{\vec{Q}}^e - \Omega_j), \quad (5.6)$$

we find the total number of daughter particles produced as a function of time $n_e(t) = \sum_{\vec{Q}} n_e(\vec{Q}, t)$ is given by

$$n_e(t) = \left[\Gamma_1 \cos^2 \theta + \Gamma_2 \sin^2 \theta \right] t, \quad (5.7)$$

where $\Gamma_{1,2}$ are the partial widths given by (4.11). In the rate (5.5), there is *no interference* between the mass eigenstates since $|\nu_{1,2}\rangle$ are orthogonal. It is straightforward to confirm that

$$n_e(t) = {}^{(1)}\langle \Psi_e(t) | \Psi_e(t) \rangle^{(1)} = \sum_{\vec{Q}} \langle \mathcal{V}_e(\vec{Q}, t) | \mathcal{V}_e(\vec{Q}, t) \rangle, \quad (5.8)$$

a result that will play an important role below.

The calculation of the parent population is slightly more involved. Since the first order state does not have any parent particle W , we must consider the second order state (5.3). To second order, there are several contributions, but the only one that is relevant is the process in which the first vertex at (\vec{x}_2, t_2) annihilates the initial W creating the intermediate state with one (e, ν_e) entangled pair, while the second interaction vertex at (\vec{x}_1, t_1) *annihilates* this (e, ν) pair in the intermediate state and creates the W , which has non-vanishing overlap with $|W\rangle$. This process is depicted in Fig. (7) and is recognized as the self-energy of the parent particle.

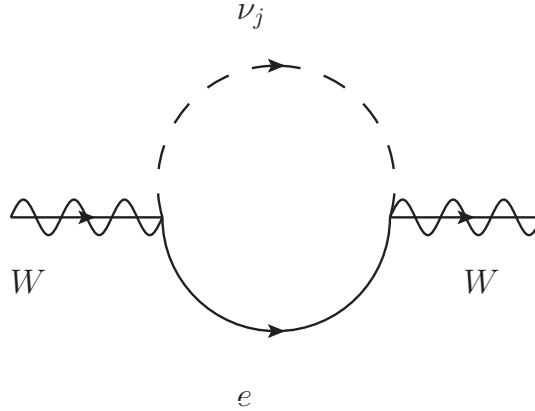


FIG. 7: Self-energy of the parent particle W

Thus to lowest order in g ,

$$N_W(\vec{k}, t) = 1 + 2 \operatorname{Re} \left[\langle W | \Psi_e(t) \rangle^{(2)} \right]. \quad (5.9)$$

It proves more convenient to calculate $dN_W(\vec{k}, t)/dt$, for which we find⁴

$$\frac{dN_W(\vec{k}, t)}{dt} = -\frac{2g^2}{8E_k^W} \int \frac{d^3\vec{Q}}{(2\pi)^3 E_Q^e} \left\{ \frac{\cos^2 \theta}{\Omega_1} \frac{\sin \left[(E_k^W - E_Q^e - \Omega_1)t \right]}{(E_k^W - E_Q^e - \Omega_1)} + \frac{\sin^2 \theta}{\Omega_2} \frac{\sin \left[(E_k^W - E_Q^e - \Omega_2)t \right]}{(E_k^W - E_Q^e - \Omega_2)} \right\}. \quad (5.10)$$

In the long time limit this becomes

$$\frac{dN_W(\vec{k}, t)}{dt} = -\left[\Gamma_1 \cos^2 \theta + \Gamma_2 \sin^2 \theta \right]. \quad (5.11)$$

Clearly, $dN_W(\vec{k}, t)/dt = -dn_e(t)/dt$ as the decay of the parent population results in the growth of the daughter population with the same rate. This is a consequence of unitarity and we can see this by substituting (5.8,5.9) into the unitarity condition

$$\langle W(\vec{k}) | U^\dagger(t, 0) U(t, 0) | W(\vec{k}) \rangle = 1 = 1 + {}^{(1)}\langle \Psi_e(t) | \Psi_e(t) \rangle^{(1)} + 2 \operatorname{Re} \left[\langle W | \Psi_e(t) \rangle^{(2)} \right] + \mathcal{O}(g^3) + \dots \quad (5.12)$$

The interpretation of (5.11) in terms of the Feynman diagram (7) also makes the conclusion of lack of interference manifest. The decay rate is the imaginary part of the self-energy. Since the correct propagating degrees of freedom are the neutrino *mass eigenstates*, the self-energy is the *sum* of the self-energy diagrams with the neutrino mass eigenstates propagating inside the loop. Therefore, it simply follows that the total decay width is the *sum* of the partial decay widths on the mass eigenstates without interference. The real time calculation presented above confirms this result directly from the evolution of the parent and daughter populations.

Thus, we confirm the analysis of Refs. [25, 26, 39, 41] that there is *no interference* of mass eigenstates and we conclude that the GSI anomaly *cannot* be explained in terms of the interference of mass eigenstates in the decay.

However, the expression (5.4) for the distribution function of the parent particle and its production rate (5.5) suggests an *intriguing* phenomenon of interference and oscillations in the *square* of the decay rate, namely

$$\left(\frac{dn_e(\vec{Q}, t)}{dt} \right)^2 \propto \left\{ \left(\frac{\cos^2 \theta}{\Omega_1} \right)^2 t \delta(E_k^W - E_Q^e - \Omega_1) + \left(\frac{\sin^2 \theta}{\Omega_2} \right)^2 t \delta(E_k^W - E_Q^e - \Omega_2) + \frac{\sin^2 2\theta}{2\Omega_1\Omega_2} \frac{\sin 2\Delta t}{2\Delta} \left[\delta(E_k^W - E_Q^e - \Omega_1) + \delta(E_k^W - E_Q^e - \Omega_2) \right] \right\}, \quad (5.13)$$

where $2\Delta = \Omega_2 - \Omega_1$ is the energy difference between the mass eigenstates. While the interference and oscillatory phenomenon in the *square* of the production rate of the daughter particle is intriguing and perhaps can be interpreted as a *fluctuation* in the production rate, it is not clear to us that the GSI anomaly is a manifestation of this phenomenon.

⁴ Effectively, we are obtaining the Boltzmann equation for the parent particle, neglecting the build-up of the population.

VI. CONCLUSIONS AND DISCUSSIONS

In this article we study the dynamics of mixing and oscillations in quantum field theory directly in real and finite time. The setting is a bosonic model that reliably describes charged current-weak interactions. This allows us to extract the relevant aspects without the peripheral complications associated with spinors. We begin by obtaining the in-out transition amplitudes and probabilities in a long but finite time interval for appearance and disappearance processes and compare these to the S-matrix results. To illustrate the effects of the finite time interval, we consider the simplest setting with plane wave states, discussing how a wave-packet treatment needs to be modified to include the finite time contributions. We find finite time contributions that display the oscillatory behavior resulting from the interference of mass eigenstates and show that these corrections can be of the same order of or larger than the S-matrix result for *appearance* experiments. A deeper analysis of the different contributions lead us to argue that the in-out treatment is ill-suited to describe long-baseline experiments. The main reason is that in the production vertex at the source or near detector, the neutrino is produced in an *entangled state* with the charged lepton.

If the charged lepton (or daughter particle) produced at the near detector is not measured, tracing out this degree of freedom yields a density matrix for the neutrino. The off-diagonal density matrix elements in the mass basis are a measure of coherence and show distinctly the oscillatory interference effects. Diagonal and off diagonal matrix elements are of the same order of magnitude during time scales $t \lesssim t_{osc} \simeq 2E/\delta m^2$, with E the typical neutrino energy, revealing that coherence survives during the time scale t_{osc} .

The measurement of the charged lepton at the near detector *disentangles* the neutrino state, and it is the further time evolution of this disentangled state with the interaction Hamiltonian that leads to the production of charged leptons at the far detector. Thus, the process of production and detection in long-baseline experiments involves *two different time scales*: the measurement of the charged lepton at the near detector determines the first time scale at which the neutrino state is disentangled, while the measurement of the charged lepton at the far detector is the second and longer time scale.

We obtain the charged lepton event *rate* at the far detector and show explicitly the conditions for the factorization of this rate into a product of the number of charged lepton events per phase space at the near detector times the *quantum mechanical* transition probability, times the differential production rate at the far detector. This factorization is a direct consequence of the *disentanglement* of the neutrino state at the near detector along with the approximation that the density of final states is a smooth function and for large energies, it is not sensitive to the energy difference of the mass eigenstates. This factorization was *assumed* in Ref. [22] and physical arguments were proposed for its validity in Ref. [21]. However, in this article, we show that the time evolution of the disentangled neutrino state unambiguously leads to the factorization, under the approximations discussed above. We would like to emphasize that the factorization in terms of the quantum mechanical probabilities is only valid for the event *rate* at the far detector. It is *not* valid for the total number of events. This latter quantity is also factorizable, but not in terms of the transition probability, but its time integrated version, which leads to a *different energy dependence of the oscillatory terms* as can be gleaned from the second lines in Eqs. (4.29,4.30). This latter fact *may* have phenomenologically important consequences in the interpretation of oscillation data.

The form of the amplitudes (3.34,3.35) and probabilities (3.36,3.37) obtained from the in-

out formulation are fundamentally different from those obtained from the time evolution of the disentangled state (4.24, 4.25). We can see why this is so by noticing the difference in how and when the interaction vertices act on the state. In the transition amplitudes (3.34, 3.35), the second order matrix element involves the time ordered product or alternatively the nested time integrals (see 3.40), which result in overall energy conservation. On the other hand, in the amplitudes obtained from the disentangled state, the perturbation acts at different and non-overlapping times. A first order vertex creates and evolves the entangled state until the measurement of the charged lepton disentangles the neutrino state, while *another* first order vertex propagates the disentangled neutrino and creates the final charged lepton that is measured at the far detector.

There is another way to understand this. As made explicit by time dependent perturbation theory (see subsection III C), there are *two* contributions (corresponding to the time ordering) whose sum yields the in-out amplitudes. These contributions are also manifest in the in-out probabilities. Whereas in the second case, there is only one contribution (as discussed in subsection III C).

These differences explain the fundamentally different form between the amplitudes and probabilities obtained from the in-out formulation, even at finite time, and those obtained from the disentanglement at the near detector and further evolution of the neutrino that leads to the charged lepton at the far detector.

Although our study has been carried out in terms of plane waves, we can extrapolate our results to include the case of wave packets. Let us consider the initial state in (4.2). Instead of being the plane wave Fock state $|W(\vec{k})\rangle$, let it be the localized state $|\widetilde{W}(S)\rangle$ given by (2.11). Let us also assume that the charged lepton measured at the near detector is measured with a wave-function represented by a wave-packet (2.11) $|\widetilde{l}_e(S)\rangle$, with *macroscopic* localization length of the order of the size of the detector. The neutrino is therefore disentangled into a wave-packet state, obtained from (4.14) by the convolution with the wave-packets of the W and e . This resulting state will be described by a wave packet whose localization length is of the order of the size of the near detector. Upon further time evolution, this wave packet will spread and split into the two mass eigenstates and produce the final charged lepton and W . The two mass eigenstates are also going to be described as wave packets. It is only when these wave packets begin to overlap with the far detector that the charged lepton at the far detector will be measured. The corresponding amplitudes will be non-vanishing when $t_D - t_S$ is of the order of the baseline, with uncertainties of the order of the size of the far detector. These mildly localized wave packets lead to both momentum and energy uncertainty of the same order $\Delta E \sim \Delta p \sim \hbar/\sigma \sim \hbar/t_S \sim 10^{-7}$ eV. These uncertainties in energy and momentum are *much larger* than typical values for the neutrino energy differences $\delta m^2/\overline{\Omega} \sim 10^{-12}$ eV. Although at this stage this discussion is based on simple physical arguments, we expect to report on a full space-time picture of this process in terms of wave-packets in forthcoming work.

The results discussed above led us to study the GSI anomaly by directly obtaining the decay rate of a parent and production rate of a daughter particle, bypassing the issue of whether amplitudes or probabilities for mass eigenstates must be summed. We show that these rates *do not feature* oscillations arising from the interference of mass eigenstates in the final state. We provide an alternative field theoretical explanation in terms of the imaginary part of the self-energy diagram of the parent particle. *However*, we find the intriguing result that the *square* of the production rate of the daughter particle *does* feature oscillations. We tentatively interpret this as a time dependent fluctuation of the rate, but its connection to

the GSI anomaly remains to be elucidated, an aspect worthy of further consideration.

In this article, we have introduced the two time measurement approach by considering the simplest model for neutrino oscillation. It would be interesting to apply this method to the more sophisticated models. A particularly interesting model is the $2 + \bar{1}$ model of [48], which features an unparticle sterile neutrino, the *unsterile* neutrino, along with the two active ones. The unparticle nature of the unsterile neutrino results in four momentum dependent mixing angles and non-trivial spectral densities of the neutrino mass eigenstates. Therefore, the quantum mechanical approach to the model of [48] can only be thought of as a proxy description and to understand its oscillation dynamics, the quantum field theoretical two time measurement approach is necessary.

-
- [1] C. W. Kim and A. Pevsner, *Neutrinos in Physics and Astrophysics*, (Harwood Academic Publishers, USA, 1993).
 - [2] R. N. Mohapatra and P. B. Pal, *Massive Neutrinos in Physics and Astrophysics*, (World Scientific, Singapore, 2004).
 - [3] M. Fukugita and T. Yanagida, *Physics of Neutrinos and Applications to Astrophysics*, (Springer-Verlag Berlin Heidelberg 2003).
 - [4] L. Wolfenstein, Phys. Rev. D **17**, 2369 (1978); S. P. Mikheyev and A. Yu. Smirnov, Sov. J. Nucl. Phys. **42**, 913 (1985).
 - [5] J. N. Bahcall, *Neutrino Astrophysics*, (Cambridge University Press, NY. 1989).
 - [6] W. C. Haxton, Ann. Rev. Astron. Astrophys. **33**, 459 (1995) [arXiv:hep-ph/9503430]; arXiv:nucl-th/0004052.
 - [7] W. Grimus, Lect. Notes Phys. **629**, 169 (2004) [arXiv:hep-ph/0307149].
 - [8] B. Kayser, arXiv:0804.1497 [hep-ph]; arXiv:0804.1121 [hep-ph].
 - [9] R. N. Mohapatra *et al.*, Rept. Prog. Phys. **70**, 1757 (2007) [arXiv:hep-ph/0510213]; arXiv:hep-ph/0412099.
 - [10] A. de Gouvea, arXiv:0902.4656 [hep-ph]; Mod. Phys. Lett. A **19**, 2799 (2004) [arXiv:hep-ph/0503086]; arXiv:hep-ph/0411274.
 - [11] C. Giunti, C. W. Kim, *Fundamentals of Neutrino Physics and Astrophysics*, (Oxford University Press, Oxford, 2007).
 - [12] W. C. Haxton, arXiv:0808.0735 [nucl-th].
 - [13] A. D. Dolgov, Surveys High Energ. Phys. **17**, 91 (2002) [arXiv:hep-ph/0208222]; Phys. Rept. **370**, 333 (2002) [arXiv:hep-ph/0202122].
 - [14] E. K. Akhmedov and A. Y. Smirnov, Phys. Atom. Nucl. **72**, 1363 (2009) [arXiv:0905.1903 [hep-ph]].
 - [15] B. Kayser, Phys. Rev. D **24**, 110 (1981); Nucl. Phys. Proc. Suppl. **118**, 425 (2003) [arXiv:hep-ph/0306072].
 - [16] J. Rich, Phys. Rev. D **48**, 4318 (1993).
 - [17] M. Nauenberg, Phys. Lett. B **447**, 23 (1999) [Erratum-ibid. B **452**, 434 (1999)] [arXiv:hep-ph/9812441].
 - [18] H. J. Lipkin, Phys. Lett. B **348**, 604 (1995) [arXiv:hep-ph/9501269]; Phys. Lett. B **579**, 355 (2004) [arXiv:hep-ph/0304187]; Phys. Lett. B **642**, 366 (2006) [arXiv:hep-ph/0505141].
 - [19] H. J. Lipkin, arXiv:0905.1216 [hep-ph]; arXiv:0904.4913 [hep-ph].
 - [20] H. J. Lipkin, arXiv:0910.5049 [hep-ph].

- [21] A. G. Cohen, S. L. Glashow and Z. Ligeti, Phys. Lett. B **678**, 191 (2009) [arXiv:0810.4602 [hep-ph]].
- [22] E. K. Akhmedov and J. Kopp, arXiv:1001.4815 [hep-ph].
- [23] K. Kiers and N. Weiss, Phys. Rev. D **57**, 3091 (1998) [arXiv:hep-ph/9710289]; K. Kiers, S. Nussinov and N. Weiss, Phys. Rev. D **53**, 537 (1996) [arXiv:hep-ph/9506271].
- [24] W. Grimus and P. Stockinger, Phys. Rev. D **54**, 3414 (1996) [arXiv:hep-ph/9603430]; W. Grimus, S. Mohanty and P. Stockinger, arXiv:hep-ph/9909341; arXiv:hep-ph/9904340; Phys. Rev. D **61**, 033001 (2000) [arXiv:hep-ph/9904285]; Phys. Rev. D **59**, 013011 (1999) [arXiv:hep-ph/9807442].
- [25] C. Giunti, Found. Phys. Lett. **17**, 103 (2004) [arXiv:hep-ph/0302026]; JHEP **0211**, 017 (2002) [arXiv:hep-ph/0205014]; Mod. Phys. Lett. A **16**, 2363 (2001) [arXiv:hep-ph/0104148]; C. Giunti and C. W. Kim, Phys. Rev. D **58**, 017301 (1998) [arXiv:hep-ph/9711363]; C. Giunti, C. W. Kim and U. W. Lee, Phys. Lett. B **421**, 237 (1998) [arXiv:hep-ph/9709494].
- [26] C. Giunti, JHEP **0211**, 017 (2002) [arXiv:hep-ph/0205014].
- [27] A. Ioannisian and A. Pilaftsis, Phys. Rev. D **59**, 053003 (1999) [arXiv:hep-ph/9809503].
- [28] C. Y. Cardall, Phys. Rev. D **61**, 073006 (2000) [arXiv:hep-ph/9909332].
- [29] M. Beuthe, Phys. Rev. D **66**, 013003 (2002) [arXiv:hep-ph/0202068].
- [30] A. D. Dolgov, O. V. Lychkovskiy, A. A. Mamonov, L. B. Okun and M. G. Schepkin, Eur. Phys. J. C **44**, 431 (2005) [arXiv:hep-ph/0506203]; A. D. Dolgov, O. V. Lychkovskiy, A. A. Mamonov, L. B. Okun, M. V. Rotaev and M. G. Schepkin, Nucl. Phys. B **729**, 79 (2005) [arXiv:hep-ph/0505251]; A. D. Dolgov, L. B. Okun, M. V. Rotaev and M. G. Schepkin, arXiv:hep-ph/0407189.
- [31] C. M. Ho and D. Boyanovsky, Phys. Rev. D **73**, 125014 (2006) [arXiv:hep-ph/0604045].
- [32] B. D. Keister and W. N. Polyzou, arXiv:0908.1404 [hep-ph].
- [33] M. Ellis and F. J. P. Soler, Nucl. Instrum. Meth. A **569**, 127 (2006).
- [34] J. M. Losecco, arXiv:0912.0900 [hep-ph]; arXiv:0902.2752 [hep-ph].
- [35] R. S. Raghavan, arXiv:hep-ph/0511191; arXiv:hep-ph/0601079.
- [36] S. M. Bilenky, F. von Feilitzsch and W. Potzel, J. Phys. G **35**, 095003 (2008) [arXiv:0803.0527 [hep-ph]].
- [37] E. K. Akhmedov, J. Kopp and M. Lindner, J. Phys. G **36**, 078001 (2009) [arXiv:0803.1424 [hep-ph]]; JHEP **0805**, 005 (2008) [arXiv:0802.2513 [hep-ph]].
- [38] C. Giunti, Phys. Lett. B **665**, 92 (2008) [arXiv:0805.0431 [hep-ph]]; arXiv:0801.4639 [hep-ph].
- [39] H. Burkhardt, J. Lowe, G. J. . Stephenson, T. Goldman and B. H. J. McKellar, arXiv:0804.1099 [hep-ph].
- [40] H. Kienert, J. Kopp, M. Lindner and A. Merle, J. Phys. Conf. Ser. **136**, 022049 (2008) [arXiv:0808.2389 [hep-ph]].
- [41] M. Peshkin, arXiv:0804.4891 [hep-ph].
- [42] Yu. A. Litvinov *et al.*, Phys. Rev. Lett. **99**, 262501 (2007) [arXiv:0711.3709 [nucl-ex]]; Phys. Lett. B **664**, 162 (2008) [arXiv:0801.2079 [nucl-ex]].
- [43] P. Kienle, Nucl. Phys. A **827**, 510C (2009).
- [44] A. N. Ivanov, R. Reda and P. Kienle, arXiv:0801.2121 [nucl-th]; A. N. Ivanov and P. Kienle, Phys. Rev. Lett. **103**, 062502 (2009) [arXiv:0908.0877 [nucl-th]]; A. N. Ivanov, E. L. Kryshen, M. Pitschmann and P. Kienle, arXiv:0806.2543 [nucl-th].
- [45] M. Faber, arXiv:0801.3262 [nucl-th].
- [46] M. O. Scully, M. S. Zubairy, *Quantum Optics*, (Cambridge University Press, Cambridge, U.K. 1997).

- [47] D. Boyanovsky, Phys. Rev. D **76**, 103514 (2007) [arXiv:0706.3167 [hep-ph]]; D. Boyanovsky and C. M. Ho, Phys. Rev. D **76**, 085011 (2007) [arXiv:0705.0703 [hep-ph]].
- [48] D. Boyanovsky, R. Holman and J. A. Hutasoit, arXiv:0912.2093 [hep-ph].